Towards real-time tumor margin assessment in colorectal liver metastases surgery using near-infrared fluorescence-imaging

Master Thesis - Tom Dijkhuis - 17 September 2021

TOWARDS REAL-TIME TUMOR MARGIN ASSESSMENT IN COLORECTAL LIVER METASTASES SURGERY USING NEAR-INFRARED FLUORESCENCE-IMAGING

By

Dijkhuis, T.H. (Tom)

Student number: 4399927

17 September 2021

Thesis in partial fulfilment of the requirements for the joint degree of Master of Science in

Technical Medicine

Leiden University; Delft University of Technology; Erasmus University Rotterdam

---

General information

Master program	Technical Medicine, Dept. of Biomechanical Engineering, TU Delft
Project duration	December 2020 – September 2021
Location internship	Surgery (Green Light Lab), LUMC
Track	Imaging and Intervention (I&I)

Supervision

Medical supervisor	Dr. J.S.D. (Sven) Mieog
Daily & 2nd medical supervisor	Drs. O.D. (Okker) Bijlstra
Technical supervisor	Dr. ir. J. (Jouke) Dijkstra
2nd technical supervisor	Dr. ir. A. (Alexander) Broersen

Thesis committee members

Prof. Dr. ir. J. (Jaap) Harlaar (chair)	TU Delft, *Department of BioMechanical Engineering*
Dr. J.S.D. (Sven) Mieog	LUMC, *Department of Surgery*
Drs. O.D. (Okker) Bijlstra	LUMC, *Department of Surgery (Green Light Lab)*
Dr. ir. J. (Jouke) Dijkstra	LUMC, *Department of Radiology (LKEB)*
A. (Alexander) Broersen	LUMC, *Department of Radiology (LKEB)*

Abstract

Introduction

Near-infrared fluorescence (NIRF) imaging is a relatively novel development in colorectal liver metastases (CRLM) surgery which has proven to be an added value for the detection of new lesions and surgical guidance. However, new possibilities of NIRF imaging in CRLM surgery are yet to be explored. The fluorescent rim of indocyanine green (ICG) surrounding CRLM can potentially be used to predict the resection margin. By predicting the resection margin, irradical resections can be observed during surgery. Additional tissue can be removed intraoperatively, probably resulting in improved outcomes. This research describes a method to analyze the data retrieved at the Department of Pathology. The goal of this thesis is to provide a verdict on whether ICG could be used as a quantitative indicator for distance to the tumor and therefore, help the surgeon to evaluate the resection margin on-site.

Materials & Methods

Data was collected by imaging bread loaves from resected CRLM. Methods to generate data from these images, to evaluate the collected data, and to evaluate the interobserver error were described. The data were evaluated with the use of general and histogram parameters. Moreover, the data was separated four times into different groups. These groups aimed to investigate the general distribution of ICG around CRLM and the effect of tumor and patient-specific characteristics. Subsequently, the results of the data analysis were used to make a rough estimation of the expected measured fluorescence intensities during surgery.

Results

The interobserver error was 0.9 or higher (Sørensen-Dice coefficient) for 8 out of the 10 delineation pairs including three pairs with a coefficient of 0.95 or higher. However, two pairs of delineations showed coefficients of 0.566 and 0.797. 33 bread loaves were included in this research for data analysis of the general and histogram parameters. Various distributions of ICG around the tumors were found for the groups varying in tumor and patient characteristics. Moreover, differences between groups in general parameters were observed. The rough estimation of the expected measured fluorescence intensity showed a peak intensity around 5 millimeters from the tumor.

Discussion

The delineation of CRLM proved to be a reproducible operation in most of the delineations (80%). However, there is a need for ground truth delineations to examine the accuracy of delineations. Besides, the effects of chemotherapy, the location of the tumor, and the size of the tumor on the peritumoral fluorescent rim, as well as the flaws of this research were discussed.

Future recommendations

Additional research must be performed to be able to develop a method to evaluate resection margins intraoperatively. Future research should focus on the formulation of an implementation plan and the development of the database, the MeVisLab network, the resection margin prediction method, and a protocol that enables the opportunity to create ground truth delineations.

Conclusion

This study showed the potential of the use of the peritumoral fluorescent rim to develop a method that can predict resection margins of resected CRLM intraoperatively. However, additional research must be performed to accurately implement the method and to increase its accuracy.

Table of contents

Introduction

Colorectal cancer (CRC) is the fifth most common malignancy in the Netherlands with 12.900 cases in 2019 (1). Globally, CRC has the third-highest prevalence. The liver, peritoneum, and lungs are the most common sites for metastases from CRC (2). Of all CRC patients, approximately25% have synchronous or metachronous colorectal liver metastases (CRLM) (2-5). The importance of adequate treatment of CRLM is high as CRC is the cancer type third most common with metastasis being the cause of death (6). Resection is the treatment option of choice for CRLM. Besides resection, ablation and chemotherapy are other often used treatment options for CRLM (7, 8). It is not uncommon that a combination of treatments is used for the best outcome.

An important factor in the 5-year survival rate of patients with CRLM is the resection margin. Ardito *et al.* showed that patients treated with resection with R0 margins (microscopically margin-negative, tumor margin ≥ 1 mm) and pre-operative chemotherapy had a 5-year survival rate of 54.9%. Moreover, R1 resection margins (macroscopic negative but microscopically margin-positive) showed a significantly lower overall 5-year survival rate (33.7%) (9). Therefore, achieving R0 resections in CRLM patients is of great importance.

Currently, surgeons in the Leiden University Medical Center (LUMC) cannot react on irradical resection margins during the procedure as the resection margins are determined approximately one week after surgery at the Department of Pathology in the LUMC. Ideally, resection margin assessment is performed intraoperatively, enabling the surgeon to increase the margin where required. The change to an R0 resection from an R1 resection may improve oncologic outcomes.

One of the new developments in CRLM surgery is the use of the fluorescent dye indocyanine green (ICG). ICG is excited by a light source (laser, 740-800 nm), and emits light (800–860 nm) at an emission peak of 820 nm (10, 11). Originally, ICG was used for measuring liver function before liver surgery (12) as ICG is taken up by hepatocytes and excreted by the biliary system. Therefore, the decrease of fluorescence in the blood flow over time indicates liver function. Eventually, Ishizawa *et al.* discovered ICG can help identify CRLM (13). ICG accumulates around CRLM and can be visualized intraoperatively by inspecting the liver with a fluorescence camera. Near-Infrared Fluorescence (NIRF) imaging is only applied in combination with intraoperative ultrasound (IOUS) as tumors located deeper than 8-10 mm are not identifiable solely by NIRF imaging, as the light emitted from ICG penetrates around 10 mm through human tissue (11, 13). Preoperative CT and/or MRI scans are used to identify tumors before surgery. During surgery, inspection, palpation and IOUS of the liver surface are used to find additional tumors. Nonetheless, the combination of these methods cannot prevent tumors from being overlooked as the methods lack accuracy in finding small lesions (11). NIRF imaging has been proved as added value for finding preoperatively identified lesions, identification of additional lesions, and for tumor margin assessment. The combination of NIRF-guidance and IOUS showed additional lesions in significantly more patients compared to solely use of IOUS (11). Therefore, NIRF-guided surgery is standard-of-care in the LUMC. ICG is administered intravenously approximately 24 hours before surgery, leading to a typical rim-shaped fluorescence enhancement pattern around superficial CRLM (*Figure 1*) (14, 15). During surgery, a NIRF camera is used to project the fluorescence in the liver to identify CRLM. After resection, the wound bed and the resection border are inspected with the NIRF camera to identify high fluorescent regions which indicate suspected irradical resection margins. Despite the use of NIRF imaging the liver-specific

recurrence-free survival at 4 years is only 47% and the overall survival 62% (11).

The fluorescence intensity of ICG around the CRLM can be used intraoperatively as an indicator for resection margins, ultimately leading to a decrease in R1 resections. This will lead to an increase in the overall survival. A prediction of resection margins can be made during surgery with NIRF imaging with the use of ICG, enabling the surgeon to increase the resection margins if necessary. However, before the fluorescence intensity of ICG can be used to define resection margins, the effect of cauterization on the measured fluorescence intensity needed clarification. As cauterization has a potential effect on the liver tissue, tumor tissue, and the fluorescence intensity of ICG. A literature review aimed to give a better understanding of the effect of cauterization on the measured fluorescence intensities during surgery was written as preparation for this thesis.

Cauterization devices 'cut and burn' through liver tissue. The 'burn' mode is used to decrease the amount of blood loss of patients, as small blood vessels are simply sealed with the device (16). However, the use of cauterization to resect CRLM could potentially influence the complexity of the prediction of the resection margin. During cauterization, tissue temperature increases to a level where tissue damage occurs. Consequently, the structure of tissue changes, leading to a change in optical properties. The scatter and absorption coefficient of the tissue will increase and will cause a decrease in the distance photons can travel through the tissue. Besides the change in tissue due to cauterization, the increase in temperature during cauterization influences the degradation of ICG. However, the effect of the temperature rise is believed to be far below the effect of tissue damage. The exact effect of cauterization on tissue and fluorescence depends on the cauterization device and the settings of the device used.

When the measured fluorescence intensity can be compensated for the exact effects of cauterization during surgery, the use of the fluorescent rim around CRLM is a promising technique to evaluate resection margins. Therefore, the exact effects of cauterization by using varying cauterization devices used at varying settings combinations still must be examined. However, the effects of cauterization are not expected to prevent the fluorescent rim to be used to evaluate resection margins.

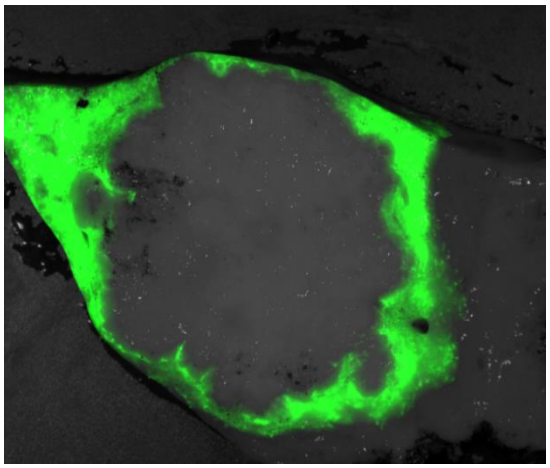

***Figure 1** - Fluorescence rim of ICG around a CRLM*

This research describes a method to analyze the data retrieved at the Department of Pathology. This method will provide insights into the distribution of ICG around CRLM, the effect of tumor and patient characteristics such as size of the tumor and preoperative chemotherapy. The goal of this thesis is to provide a verdict on whether ICG could be used as a quantitative indicator for distance to the tumor and therefore, help the surgeon to evaluate the resection margin on-site.

Materials

This study was approved by the Dutch Medical-ethical Committee Leiden, Delft, Den Haag, with study number B19.056. The materials used in this research were possessed by the LUMC or freely available online. For obtaining data from the resected metastases the PEARL Trilogy Small Animal imaging system (LI-COR Biotechnology, Lincoln, Nebraska USA) was used. This system was used to make both white light images as fluorescence images at 800nm. MeVisLab version 3.4.1 (MeVis Medical Solutions AG and Fraunhofer MEVIS – Institute for Medical Image Computing), QuPath (17), and Excel (Microsoft Windows) were used for data processing and data analysis. ImageJ was used to visualize the distribution of fluorescence around the CRLM.

Methods

Sample/Data collection

Directly after surgery, the resected metastases were collected and transported to the Department of Pathology. First, an image of the complete specimen was made, when possible, with the PEARL. On the resection border, ink was applied so the resection border could be identified when the sample was cut in bread loaves. The sample was prepared for imaging with the PEARL by cutting the sample in bread loaves of +/- 0,5 to 1 centimeter in width. The bread loaves were imaged on both sides with the PEARL. The settings used with the PEARL can be found in *Table 1*. After imaging, the bread loaves were taken by the pathologist and prepared for microscopic analysis (*Figure 2*).

Table 1 *- Settings of the PEARL imaging system*

Parameter	Setting
Resolution	85 µm (300 dpi*)
Wavelengths	White light & 800 nm
Focus	-2
Image size	1300 x 964 pixels

* dpi = dots per inch

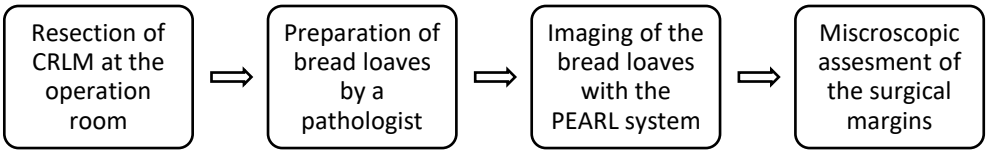

Figure 2 *- Flowchart of the route of resected samples*

Image generation

The collected PEARL images were used for generating data which was performed in MeVisLab. However, before data could be generated in MeVisLab, QuPath was used to make several other types of images. The different types and specifications of these images can be found in *Table 2*. The bread loaves and tumors were delineated manually in QuPath by interpreting the intensity values. Several bread loaves could be imaged at the same time in the PEARL as multiple bread loaves, depending on the size of the bread loaves. To select one specific bread loaf, the delineation of tumor and bread loaf was performed separately for each bread loaf. Both the bread loaf delineations and the tumor delineations were exported separately (*Figure 3*). Both images were used as masks in MeVisLab. The fluorescence image was exported via QuPath to reorganize the intensity values of the image from the original pixel intensities to pixel intensities between 0 and 255, where 255 was the maximum fluorescence intensity in the image and the intensities were divided proportionally. This was performed for image processing purposes in MeVisLab and to be able to compare different samples with each other. Besides the intensity values between 0 and 255, the original fluorescence image was exported a second time with the original pixel values in an OME TIFF format to be able to perform calculations with the original pixel values.

Table 2 *- Specifications of the generated images in QuPath*

Image	Specification
Tumor delineation	1300 x 964 pixels 0/178/255
Bread loaf delineation	1300 x 964 pixels 0/178/255
Fluorescent image	1300 x 964 pixels 0 – 255
Fluorescent image	1300 x 964 pixels Original pixel intensities

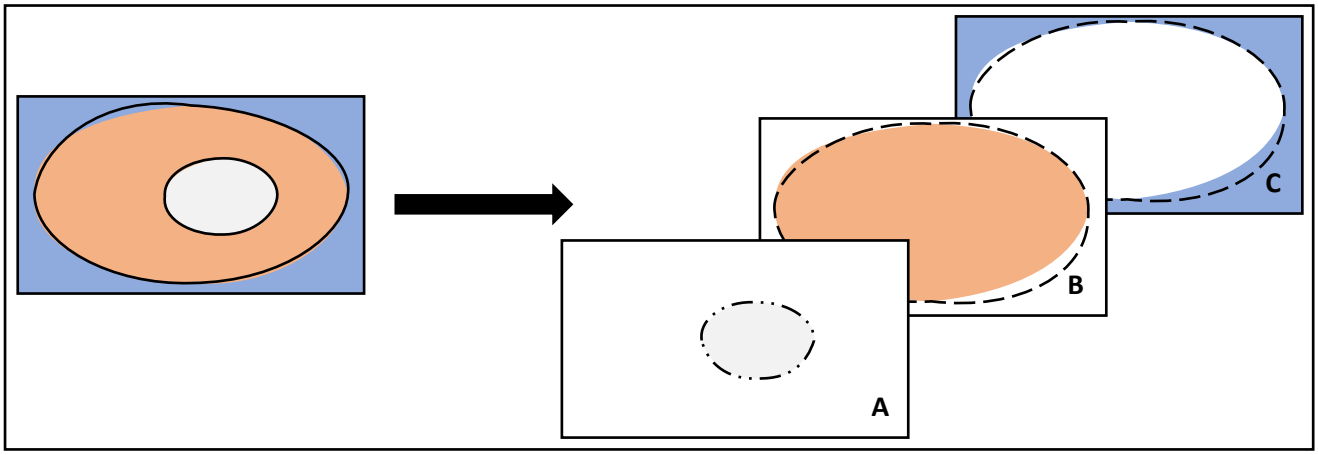

Figure 3 *- Overview of the images used to generate data*

The tumor (A) and bread loaf (B) were delineated in the original image (left) and were exported. The inverse of the bread loaf image results in an image of the background (C).

Interobserver error

The interobserver error was calculated to evaluate the accuracy of the delineation of the researcher. To calculate the interobserver error an experienced pathologist delineated 10 CRLMs in bread loaves. Simultaneously, the researcher, who delineated all CRLMs for this research, delineated the same CRLMs. The delineations were then compared with each other. The Sørensen-Dice coefficient was used to evaluate the interobserver error. The Sørensen-Dice coefficient is as follows:

Equation 1 *- Sørensen-Dice coefficient*

$$DSC = 2 * \frac{|X \cap Y|}{(|X| + |Y|)}$$

Where,

DSC = The Sørensen-Dice index

X = Image 1

Y = Image 2

The Sørensen-Dice coefficient measures the similarity between two images. $|X \cap Y|$ is the number of overlapping pixels between the two images X and Y. $|X|$ is the number of pixels of which image 1 exists and $|Y|$ of which image Y exists.

After completing the delineations of the CRLMs, all delineations were manually checked and evaluated by the pathologist. Both the pathologist and researcher delineated CRLMs in images generated with the PEARL imaging system in QuPath for the first time. Therefore, the delineations of the researcher could not be compared with a 'ground truth' image.

MeVisLab structure

MeVisLab was used to extract data from the images generated in QuPath.

Preprocessing

The delineated tumor and bread loaf images were first preprocessed. In both images, the noise was removed and converted into an image consisting of pixels with the values 1 or minus 1. The noise was removed by filtering the specific pixel intensities for noise out the image. The pre-processed image was used to be able to perform calculations with the fluorescence images. The background pixels were given the value minus 1 to be able to distinguish background pixels and pixels in the fluorescent images with a pixel intensity of 0 a.u.

Generation of the dilated images

Generation of dilated images of the tumor was performed separately for each tumor and bread loaf. The tumor delineation image was taken and dilated at varying extents. The steps taken for dilation can be found in *Table 3*. The original delineated tumor image was then subtracted from the dilated image so a halo around the tumor was produced (*Figure 4, Table 3, Table 4*). For better understanding of the distribution of ICG from the tumor border to the various halos, the halos ware subtracted from each other. This results in smaller halos at different distances from the tumor (*Table 4*). These halos were then used as a mask for the fluorescence image (0 – 255) so a halo around the tumor consisting of fluorescence data was generated. Only the subtracted halos were then used to generate data per tumor to compare the different tumors.

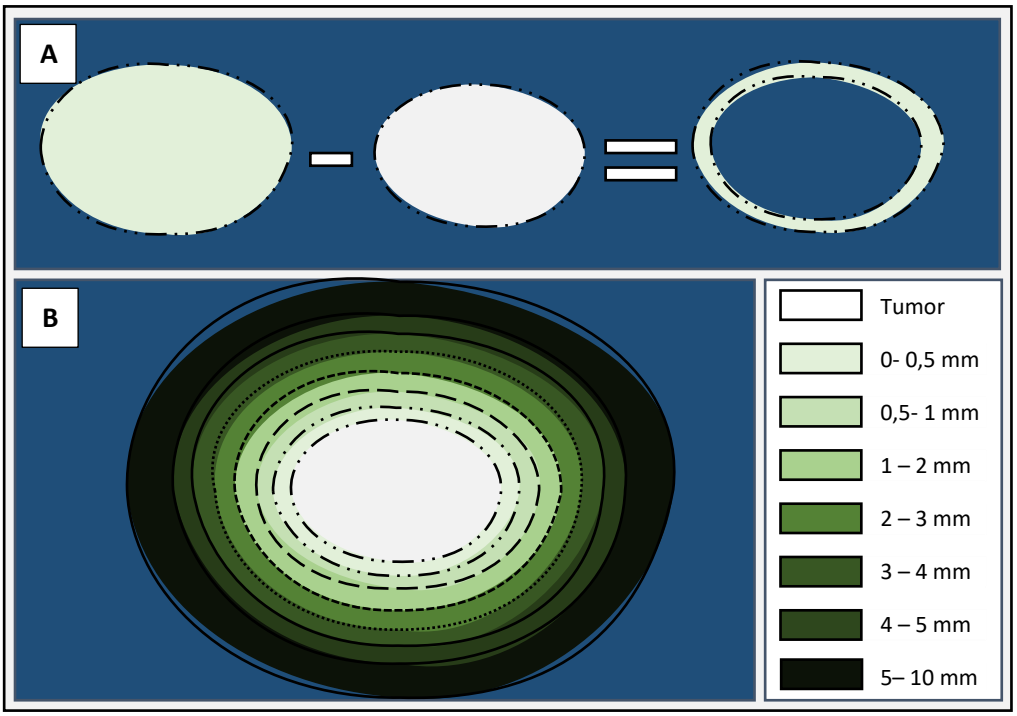

Figure 4 *- Dilation of the tumor and generation of halos*

To obtain more information about the distribution of fluorescence around the tumor, the tumor is dilated with varying extents (B). The tumor is subtracted from the dilated tumor, so a halo is generated with an open center in the shape of the tumor (A). (B) gives an overview of the different halos and how the different halos relate.

Table 3 - Distances from the borders of the dilated halos to the tumor

Dilation (mm)	Halo border distance to tumor (mm – mm)
0,5	0 – 0,5
1	0 – 1
2	0 – 2
3	0 – 3
4	0 – 4
5	0 – 5
10	0 – 10

Table 4 - Distances from the borders of the subtracted halos to the tumor

Halo border distance to tumor (mm – mm)
0 - 0,5
0,5 - 1
1 - 2
2 - 3
3 - 4
4 - 5
5 - 10

Octant generation

Octants were used as a method to provide a better understanding of the distribution of the fluorescence around the tumor on bread loaf images. Octants were used instead of quadrants as octants can give more information about the fluorescence intensity gradient from the liver border to the resection border. The dimensions of the octants were calculated by calculating a bounding box around the tumor. The bounding box shows a border around the tumor in which all data points of the tumor are located (*Figure 5*). Subsequently, the center of mass of the tumor was determined. Since tumors can have irregular shapes, the center of mass was not necessarily the geometric middle of the tumor. The center of mass was used in this research as the center of mass is the point of rotation of the tumor. The center of mass was then used as the intersection of the middle four octants. The distance between the center of mass and the borders of the bounding box were then calculated. One centimeter was then added to the highest distance between the center of mass and the border of the bounding box in the vertical and horizontal direction. So, that a symmetric box around the center of mass was generated (*Figure 5*). The box is divided into 4 equal parts between the liver border and the resection edge (horizontal direction in *Figure 5*) to gain more knowledge about the distribution of ICG when going deeper into the liver. In the other direction (vertical direction in *Figure 5*) the box was divided into 2 equal parts. The points were connected, so the equally shaped octants were generated.

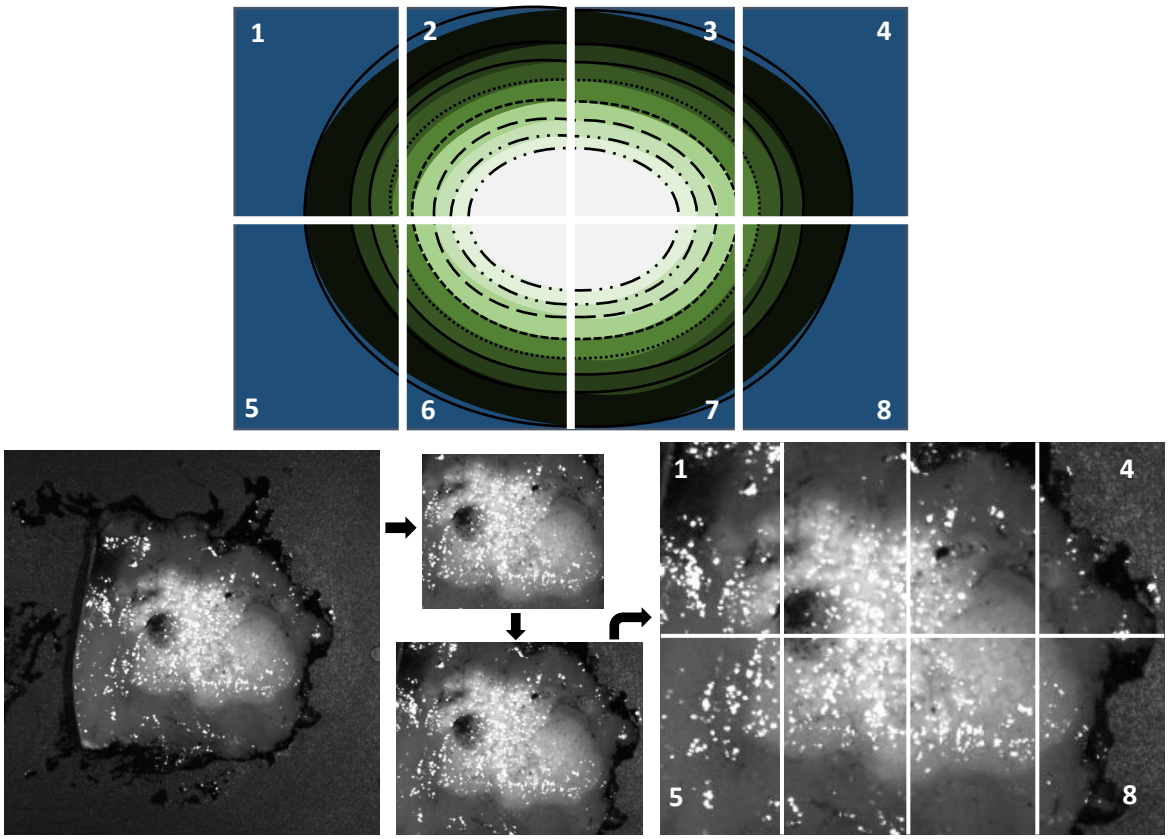

Figure 5 *- Generation of the octants*

The image of the whole bread loaf (left) was used to generate the octants. In this image, the liver border is on the left in all images. A bounding box was then applied around the tumor (upper middle). The bounding box was then dilated. This results in the image (lower middle) which was used to generate the octants. The octants were generated in the same way for every bread loaf. The octants are numbered 1 to 8. Octants 1 to 4 are on the upper row of the image and octants 5 to 8 are on the lower row. Where octants 1 and 5 lay on the left side of the image where the capsule of the liver lays. Octants 4 and 8 lay on the right side of the image and always lay at the deep side of the liver. Octants 2, 3, 6, and 7 lay around the center of the tumor.

Outcomes

General parameters

For every octant and the subtracted halos, several generic parameters were determined. The outcomes are found in *Table 5*. For every tumor, the background fluorescence intensity of the liver was determined. The background fluorescence intensity of the liver was determined by calculating the mean fluorescence intensity in the whole bread loaf without tumor tissue. Besides the background fluorescence intensity of the liver, the background fluorescence intensity in the tumor was used as an outcome. The fluorescence in the tumor was determined by calculating the mean fluorescence intensity over an area of 10 x 10 pixels at the center of mass of the tumor. A smaller area was chosen as bread loaves are three-dimensional. Therefore, ICG could be present underneath the surface. This could have a significant effect on the mean fluorescence when calculating the mean fluorescence in the whole tumor. The parameters mentioned above were named the 'general parameters' in this research. Moreover, the size of the tumor was determined**.** The minimum and maximum intensity values of the original pixel intensity images were calculated and exported. These values could be used to perform calculations to rescale the fluorescent images. All outcomes were calculated automatically. Therefore, no corrections for errors were made during the data generation.

Histogram parameters

Histograms were made for every subtracted halo for every octant (*Table 4*). This was performed for every octant separately. The parameters determined from these histograms are found in *Table 5*. All histogram parameters were calculated for every histogram of all subtracted halos in all octants. All histogram parameters had values between 0 and 255.

Table 5 *- Outcomes of the MeVisLab network*

Parameter	Calculated from
Background fluorescence (liver)	Bread loaf minus tumor, fluorescence (0-255)
Background fluorescence (tumor)	10 x 10 pixels at center of mass, fluorescence (0-255)
Size tumor	Tumor
Minimum	Bread loaf minus tumor (OPFI*)
Maximum	Bread loaf minus tumor (OPFI*)
Mean	All Histograms
Median (Q50)	All Histograms
Non-zero minimum	All Histograms
Non-zero maximum	All Histograms
Confidence interval	All Histograms
Q25	All Histograms
Q75	All Histograms

** OPFI – Original pixels fluorescence image*

Overview of the network

A simplified overview of the network is found in *Figure 6*.

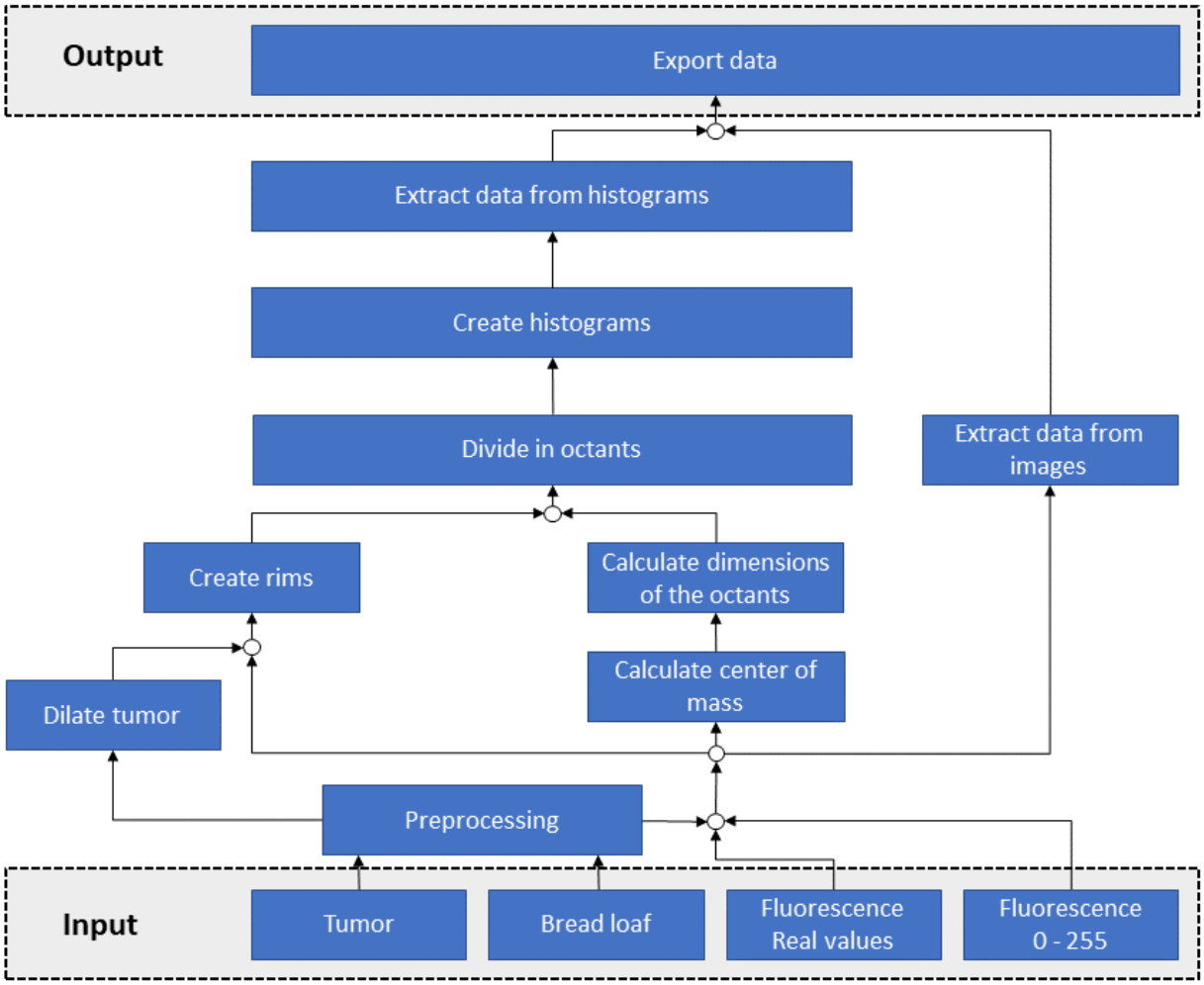

Figure 6 *- MeVisLab network*

This figure gives a simplified overview of the MeVisLab network used to generate data. As input for the network, images of the delineated tumor, delineated bread loaf, fluorescence image with real intensity values, and fluorescence image with intensity values between 0 and 255 were used. At first, the delineated tumor and bread loaf images were pre-processed. The tumor image was then dilated and used together with the fluorescence image (0-255), the bread loaf image, and the non-dilated tumor image to generate halos. To divide the halos in octants the tumor image was used again to calculate the center of mass. Followed by calculations to determine the dimensions of all octants. All halos were then divided into the octants from which histograms are made. From these histograms, several parameters were extracted. These parameters were exported to Excel together with the general parameters of all four input images.

Data analysis

Microsoft Excel was used for data analysis. The data generated in MeVisLab were exported to Excel (*Table 5*). To gain more knowledge about the effect of several tumor and patient characteristics on the distribution of fluorescence around CRLM, the data was divided four times into different groups which were compared (*Table 6*).

General distribution of ICG around CRLM

The first analysis aimed to find the general distribution of ICG around CRLM for all bread loaves. Therefore, a group including all bread loaves was generated.

Effect of preoperative chemotherapy on the peritumoral fluorescent rim

The effect of preoperative chemotherapy was investigated by dividing the data into two groups. The first group was filled with bread loaves from patients who did receive preoperative chemotherapy. The second group was filled with bread loaves from patients who did not receive preoperative chemotherapy.

Effect of the location of the CRLM in the liver on the peritumoral fluorescent rim

The effect of the location of the CRLM was investigated by dividing the data into two groups. The first group was filled with bread loaves with capsular lesions. The second group was filled with bread loaves with tumors with subcapsular lesions.

Effect of the size of the CRLM on the peritumoral fluorescent rim

To analyze the effect of the size of the CRLM the bread loaves were divided into four groups. The bread loaves were divided into groups with CRLM with a size between 0-1 cm^2, 1-2 cm^2, 2-3 cm^2, and larger than 3 cm^2.

For the analysis of all comparisons to examine the effect of the different patient and tumor characteristics the same method was used. First, the general parameters were compared to find differences between the groups. P-values were calculated with the use of the unpaired two-tailed t-test to examine the significance of the differences between the groups. Eventually, the groups were compared with the use of the comparisons of image characteristics which can be found in *Table 7*. The background fluorescence intensity of the tumor, of the bread loaf, and the maximal fluorescence intensity of the image were compared to find the relation between those three image characteristics. Furthermore, the histogram parameters in *Table 5* were analyzed by comparing the histogram parameter values of all subtracted halos for all octants.

Table 6 *- Patient and tumor characteristics investigated for their effect on the peritumoral fluorescent rim*

Patient or tumor characteristic
Preoperative chemotherapy
Location of the CRLM in the liver
Size of the CRLM

Table 7 - Comparisons of image characteristics

Comparisons of image characteristics
Background fluorescence intensity of the tumor versus maximal fluorescence intensity
Background fluorescence intensity of the tumor versus background fluorescence intensity of the bread loaf
Background fluorescence intensity of the bread loaf versus maximal fluorescence intensity
Analysis of the histogram parameters per octant per halo

Propagation of fluorescence through tissue

An estimation of the propagation of fluorescence through the tissue was made to translate the data to real intraoperatively expected outcomes as the data in this research is retrieved in another plane then a surgeon would use during surgery (*Figure 7*). A systematic approach was needed to translate the data to the other plane. However, the resulting data did not have to be exact as an estimation of the proportions of the data would already provide insights if on-site evaluation of the resection margins was possible.

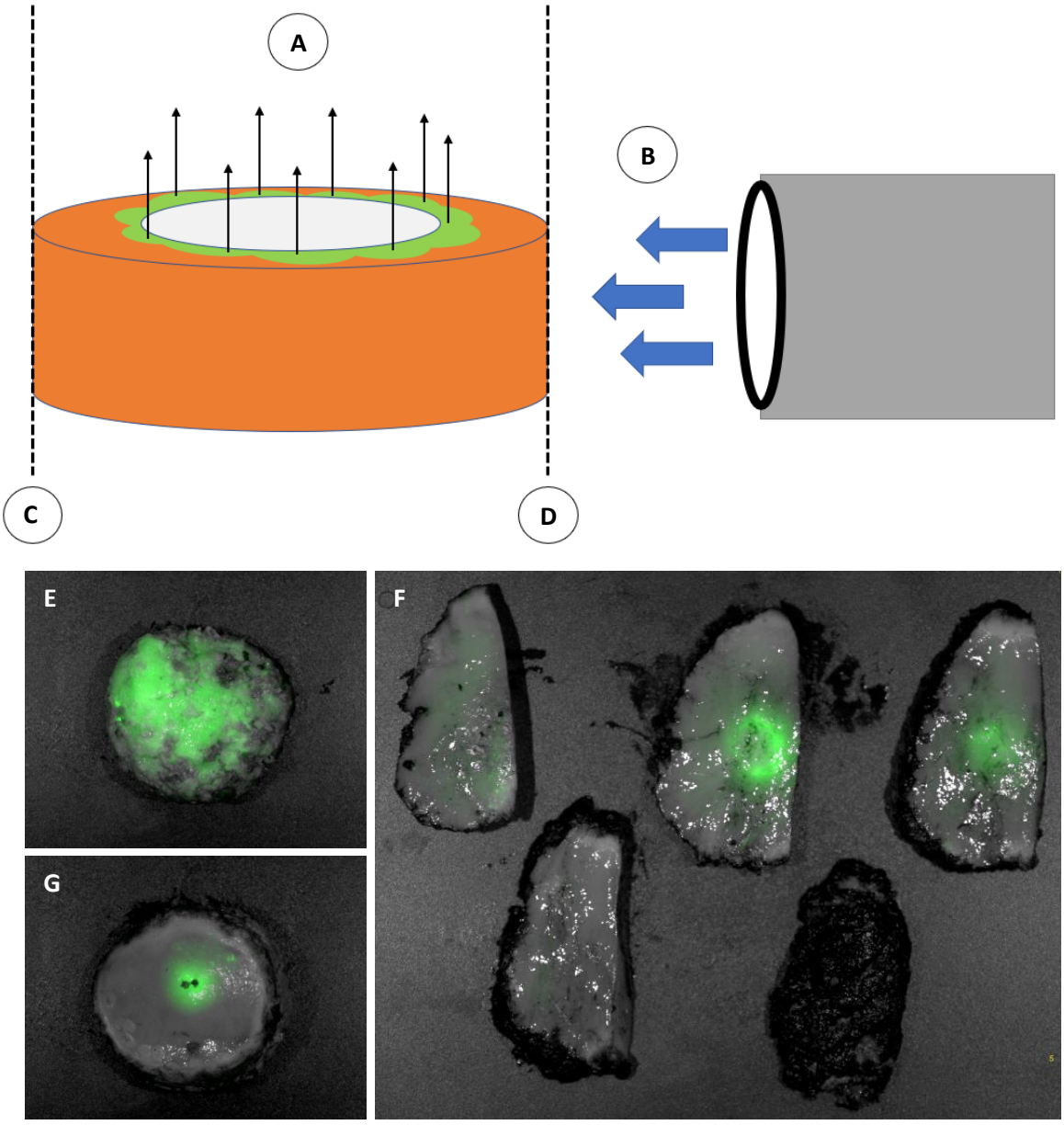

Figure 7 *- Perspective for retrieving data with the PEARL versus perspective for the surgeon during surgery*

This figure shows the difference in perspective for retrieving data and the perspective during surgery for the surgeon. (A) Shows the perspective for retrieving data. The sample was cut in bread loaves where at one end (D) lays the liver border and at the other side lays the 'inside of the liver and the resection plane (C). However, during surgery, the surgeon approaches the CRLM from outside the liver (B). This perspective lays perpendicular to the perspective during the data collection. (E) shows 'the back' of a resected CRLM. This view corresponds to the image which will be retrieved when the camera views the resected sample from side (C). (F) shows bread loaves from (E) and (G). This image corresponds with (A). (G) shows the resected CRLM from the outside of the liver and corresponds with the image resulting when the camera is positioned as showed above.

A prediction, about whether the fluorescence intensity of ICG can be used as indicator for distance to tumor, was made with the use of a formula. The formula was designed to make a rough estimation of the expected ratios between varying distance to tumor and expected measured fluorescence intensity. This specific formula could only be used for distances to the tumor of 2, 3, 4, and 5 millimeters with the generated data. The formula used is as follows:

Equation 2 *- Formula to predict the measured fluorescence intensity at various distances to the tumor*

$$F_e = 0{,}5 * \left(I_{0,5} * 0{,}5^{\frac{m-0{,}25}{TMFP}} + I_1 * 0{,}5^{\frac{m-0{,}75}{TMFP}}\right) + \sum_{i=2}^{m} I_i * 0{,}5^{(m-(i-0{,}5))/TMFP}$$

Where,

F_e *= Expected measured fluorescence intensity*

I_x *= The average fluorescence intensity in the halo up to x millimeters to the tumor*

m = Measuring distance to the tumor in mm

i = The distance of the border of the halo most far away from the tumor in mm

TMFP = Transport mean free path

A variation of the formula was used to calculate the expected measured fluorescence intensities at 0,5, 1, and 10 millimeters from the tumor. To calculate the expected measured intensity at 0,5 millimeters from the tumor $F_e = 0{,}5 * I_{0,5} * 0{,}5^{\frac{m-0{,}25}{TMFP}}$ was used. For 1 millimeter from the tumor $F_e = 0{,}5 * \left(I_{0,5} * 0{,}5^{\frac{m-0{,}25}{TMFP}} + I_1 * 0{,}5^{\frac{m-0{,}75}{TMFP}}\right)$ was used. The calculation at 10 millimeters was performed by filling in 10 millimeters at every *m* except for the *m* above the summation sign. For this *m* the value 5 must be filled in. By adding the result of $I_i * 0{,}5^{(10-(10-2{,}5))/TMFP}$ to the formula, the expected measured fluorescence intensity at 10 millimeters from the tumor was calculated. *Equation 2* made use of the average mean fluorescence intensity per halo and assumed the fluorescence was only present in the middle of the halo. Besides, the formula assumed photons only leave their initial path after a scatter event or after they were absorbed. The chance for a photon to leave its initial path was calculated by using the Transport Mean Free Path (TMFP). TMFP was described as follows:

Equation 3 *- Transport mean free path*

$$TMFP = \frac{1}{\mu_s' + \mu_a}$$

Where,

μ_s' *= Reduced scattering coefficient*

μ_a *= Absorption coefficient*

The reduced scattering coefficient was defined as $\mu_s' = \mu_s(1-g)$, where g is the anisotropy function which describes the probability of scattering in the forward direction and μ_s is the scattering coefficient. In this formula, the g-value 0,964 was used which is earlier described by Saccomandi *et al.* (18). As absorption and scattering coefficient 0,12 mm^{-1} and 2,6 mm^{-1} were used, respectively. These values were found in chicken livers for photons at the wavelength of 810nm (19)**.** Completing the formula with these values resulted in a TMFP of 4,68 mm. Therefore, the average distance a photon is expected to travel through liver tissue before leaving its initial path is 4,86 mm. *Equation 2* was formulated by the assumption 50% of the photons will leave their initial path

before 4,86 mm and 50% will leave after its initial path after 4,86 mm. The expected number of photons, which were measured at a specific distance from the tumor after traveling through the liver, was then calculated by calculating the expected number of photons that left their initial path over that specific distance.

Besides all aforementioned assumptions, the assumption that the measurements were performed directly at the surface of the bread loaf was made to eliminate interactions of photons in the air. Another important assumption that was made is that liver tissue was homogeneous. The refraction, the reflection of the light, and the measurement of scattered photons were not considered in this formula. Furthermore, the damage created during surgery, for example, damage caused by cauterization, was not considered to be able to use the scattering and absorption coefficients, as found in literature (19).

Images of 33 different bread loaves from 7 different patients were included in this research. For all bread loaves the tumor and bread loaf were delineated by the researcher. These images were exported and used for data generation and analysis.

Interobserver error

In total, 10 CRLM were delineated by the researcher and the pathologist. *Table 8* shows the results of the comparison of the delineations from the researcher and the pathologist.

***Table 8** - Differences in delineation of 10 CRLM between the researcher and the pathologist*

Tumor	Difference researcher (# pixels)	Difference pathologist (# pixels)	Combined difference (# pixels)	Overlap (# pixels)	Sørensen-Dice coefficient
1	3252	1313	4565	25469	0.918
2	4287	3916	8203	76881	0.950
3	3335	4093	7428	53357	0.935
4	279	181	460	4105	0.947
5	9	3192	3201	2090	0.566
6	738	715	1453	7322	0.910
7	245	750	995	9610	0.951
8	827	1826	2653	5194	0.797
9	5678	806	6486	59032	0.948
10	3560	1810	6370	106147	0.975

* # pixels = Number of pixels

In total, the researcher and pathologist shared 349207 overlapping pixels, which combined to an area of 25,23 cm^2 of tumor tissue. The researcher selected a total of 22210 extra pixels as tumor tissue which is comparable to 1,60 cm^2 of tumor tissue, resulting in 6,4% extra tumor tissue compared to the overlapping pixels. The pathologist selected a total of 18602 extra pixels as tumor tissue which is comparable to 1,35 cm^2 of tumor tissue, resulting in 5,3% extra tumor tissue compared to the overlapping pixels. Therefore, a mean of 1,48 cm^2 (5,8%) extra tumor tissue was selected by the pathologist and researcher. Out the 10 delineations, 80% showed a Sørensen-Dice coefficient above 0.9 including three pairs with a coefficient of 0.95 or higher. The lowest coefficients were found in tumors 5 and 8, which showed 0.566 and 0.797 as coefficients, respectively.

After completing the delineations of all tumors, all 10 pairs of delineations were manually inspected and evaluated by the pathologist. Images of tumors 5 and 8, including the delineations of the pathologist and researcher, can be found in *Figure 8*. Both tumors displayed significant differences between the delineations of the researcher and the pathologist. The pathologist could not select the correct delineation of tumor 5, as the tumor in the image showed a low contrast with the liver tissue. Tumor 8 did show a spot which the pathologist suspected of being tumor tissue. Therefore, the delineation of the pathologist of tumor 8 was expected to be more accurate. Other delineations of tumors did not show significant differences during the evaluation. However, the pathologist did observe marginal differences between all pairs of delineations. However, the correct delineation could not be identified as the exact location of the tumor borders was uncertain (*Figure 9*).

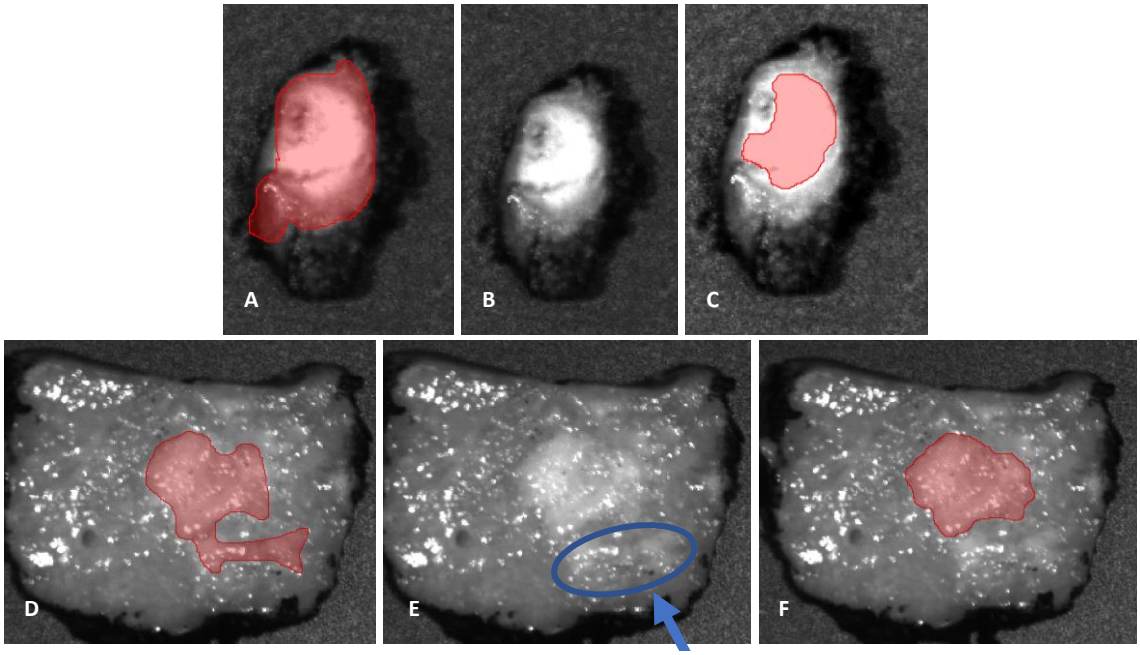

Figure 8 *- Delineations of tumor 5 and 8*

Figures (A), (B), and (C) show tumor 5. Figures (D), (E), and (F) show tumor 8. Figures (A) and (D) show the delineations of the pathologist, (C) and (F) the delineations of the researcher, and (B) and (E) the tumor without delineations. Figures (A) and (C) show significant differences between both delineations. Tumor 8 (E) shows a spot suspicious for tumor tissue (blue circle). The pathologist did identify this spot as tumor tissue (D) while the researcher (F) did not identify these pixels as tumor tissue.

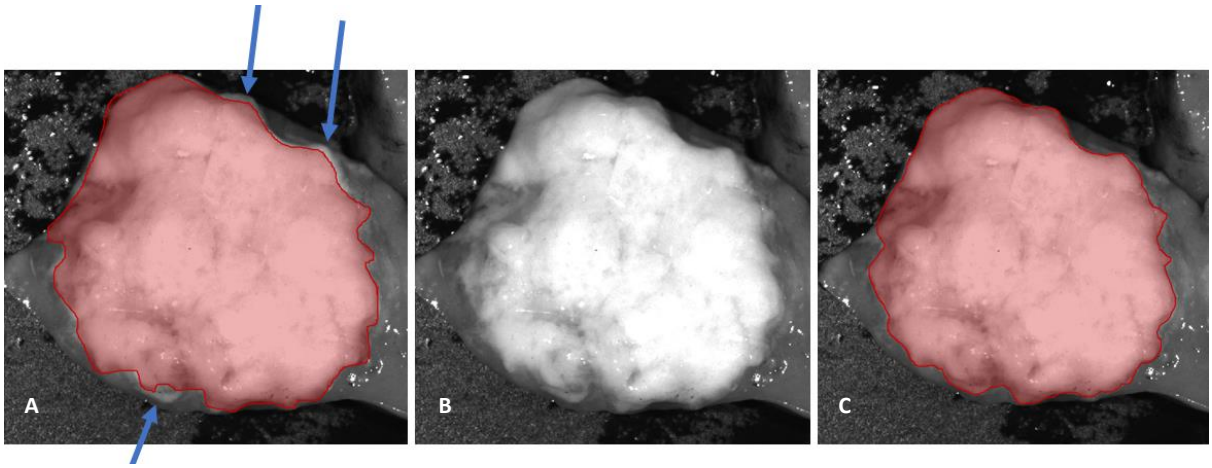

Figure 9 *- Delineations of tumor 10*

Figure (A) shows the delineation of the pathologist, figure (C) shows the delineation of the researcher, and Figure (B) shows the tumor without delineations. Marginal differences between the delineation of the researcher and the pathologist were observed. The pathologist did not select pixels as tumor tissue (blue arrows) which were found suspicious for tumor tissue during the manual evaluation of the delineations. However, the exact location of the border of the CRLM remained uncertain.

Outcomes

Histogram parameters

As displayed in *Table 5,* several parameters were extracted from histograms of equally shaped octants. However, analysis of the data from octants 1, 4, 5, and 8 showed that most of the bread loaves did miss data in these four octants. Only 3 out of the 33 bread loaves did present mean values higher than zero for all octants in the fluorescent halo of 0 to 0,5 millimeters from the tumor. In the halo of 5 to 10 millimeters from the tumor, 12 bread loaves showed usable data. As a result of the missing data, octants 1, 4, 5, and 8 were not included in the data analysis in this research. Besides, the octants in 6 bread loaves were reorganized to correct the different orientation of these 6 bread loaves compared to the other bread loaves. Octant 2 was filled with the data from octant 3, octant 3 with data from octant 7, octant 6 with data from octant 2, and octant 7 with data from octant 6.

Data analysis

General distribution of ICG around CRLM

General parameters

In total, 33 bread loaves of resected CRLM samples were included in this research. The CRLMs were resected from 7 different patients of which 5 patients received preoperative chemotherapy. In total, 21 bread loaves were exposed to chemotherapy. The mean maximal fluorescence intensity of all bread loaves was 1,79 +/- 0,98 a.u. and the mean size of the tumors 2,33 +/- 2,58 cm^2. The mean background fluorescence intensity in the tumors and the bread loaves (0-255) were 22,58 +/- 24,79 and 40,15 +/- 13,74, respectively. Both types of background fluorescence intensities showed a large spread in data (2,33 – 122,35 and 15,93 – 80,94). The characteristics of the group including all bread loaves can be found in *Table 9.*

Table 9 *- Characteristics of the group including all bread loaves*

Parameter	Mean	Min - Max
Different patients	N = 7	-
Size tumor (cm^2)	2,33 +/- 2,58 cm^2	0,02 – 11,18
Maximal fluorescence intensity (a.u.)	1,79 +/- 0,98	0,24 – 4,05
Preoperative chemo	N = 21	-
Background in tumor (0-255)	22,58 +/- 24,79	2,33 – 122,35
Background in bread loaves (0-255)	40,15 +/- 13,74	15,93 - 80,94

Background fluorescence intensity in the tumor vs maximal fluorescence intensity

The background fluorescence intensity in the tumor was compared with the maximal fluorescence in the bread loaf in arbitrary units (*Figure 10*). The background fluorescence intensity was compared to the maximal fluorescence intensity in the bread loaf in a.u. and in values between 0-255. The comparison of the background fluorescence intensity in values between 0-255 in the tumor did not show a high correlation with the maximal fluorescence intensity. The maximal fluorescence intensity showed a high spread of datapoints. Most of the datapoints (72,7% (24/33) were positioned between 0 and 25 for the background fluorescence intensity in the tumor (0-255). However, 9 datapoints were positioned outside of this range. The change of the units of the background fluorescence intensity in the tumor to a.u. did not provide additional information. The outliers farthest away from the cluster, when using the arbitrary units, did appear in bread loaves with higher maximal fluorescence intensities.

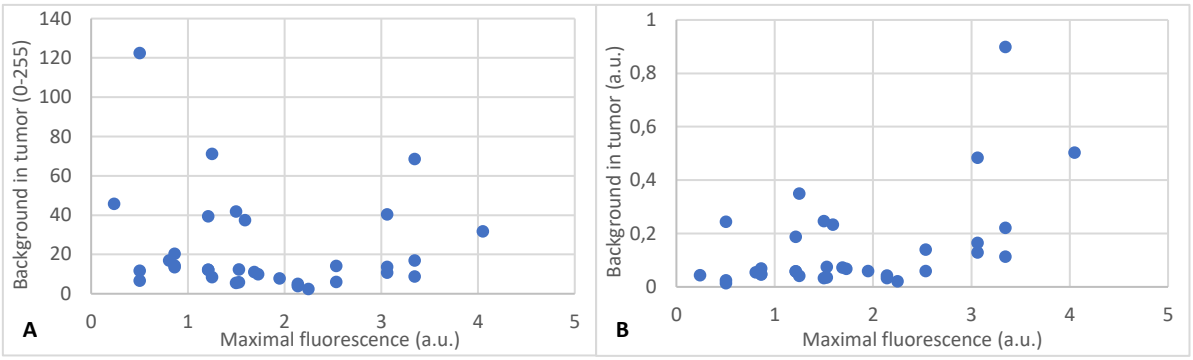

Figure 10 *- Background fluorescence intensity in the tumor versus maximal fluorescence intensity*

Figure (A) shows the background fluorescence intensity in the tumor in units between 0 and 255. Figure (B) shows the background fluorescence intensity in arbitrary units.

Background fluorescence intensity in the tumor versus background fluorescence intensity in the bread loaf

The background fluorescence intensity in the tumor and the background fluorescence intensity in the bread loaf were compared with each other using values between 0-255 (*Figure 11*). The values were not compared again while using arbitrary units as this would not provide additional information. The graph showed clustering of datapoints between 0 and 25 for the background fluorescence intensity in the tumors (0-255) and between 25 and 55 for the background fluorescence intensity in the bread loaves (0-255). However, 10 datapoints were positioned outside of this cluster. 8 of these datapoints corresponded to bread loaves with a relatively high background fluorescence intensity in the tumor, as well as in the bread loaf.

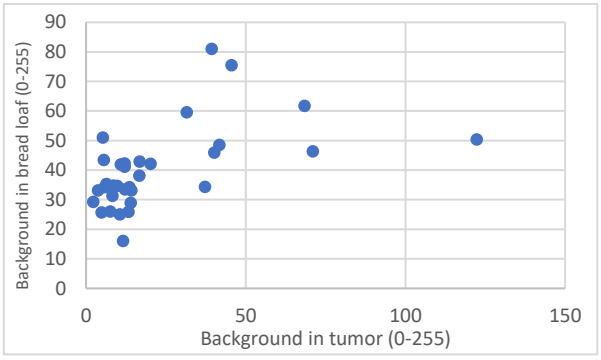

Figure 11 *- Background fluorescence intensity in the tumor versus background fluorescence intensity in the bread loaf*

Background fluorescence intensity in the bread loaf versus maximal fluorescence intensity

The graph comparing the background fluorescence intensity in the bread loaf using values between 0-255 and the maximal fluorescence intensity (*Figure 12A*) displayed a cluster of datapoints with a high spread in maximal fluorescence intensity. The spread in background fluorescence intensity in the bread loaf (0-255) was, as observed earlier, between 25 and 55. The use of the background fluorescence intensity in a.u. in the comparison with the maximal fluorescence intensity showed a correlation between both parameters (*Figure 12B)*. As displayed, an increase in the maximal fluorescence (a.u.) led to an increase in background fluorescence intensity in the bread loaf (a.u.).

Analysis of the histogram parameters per halo per octant

The results of the histogram parameters of all halos in octants 2, 3, 6, and 7 can be found in *Figure 13*. Octants 3 and 7 showed the highest 'mean', 'Q25', 'Q50', and 'Q75' values up to the halo of 4 to 5 millimeters from the tumor. For all octants, all histogram parameters of the halo of 5 to 10 millimeters from the tumor laid in a range of 20 (0-255). Octants 3 and 7 showed an increase in the values of the parameters 'mean', 'Q25', 'Q50', 'Q75', and 'non-zero minimum' until the halo of 0,5 to 1 millimeter from the tumor. The mean of these parameters decreased after the halo of 0,5 to 1 millimeter from the tumor when increasing the distance to the tumor. Octants 2 and 6 displayed the same for the parameters 'Q25' and 'non-zero minimum'.

However, octants 2 and 6 both presented the highest mean of the parameters 'mean', 'standard deviation', 'Q50', 'Q75', and 'non-zero maximum' at the halo of 1 to 2 millimeters from the tumor. Octants 3 and 7 showed the highest means at the halo of 1 to 2 millimeters from the tumor for the parameters 'standard deviation' and 'non-zero maximum'.

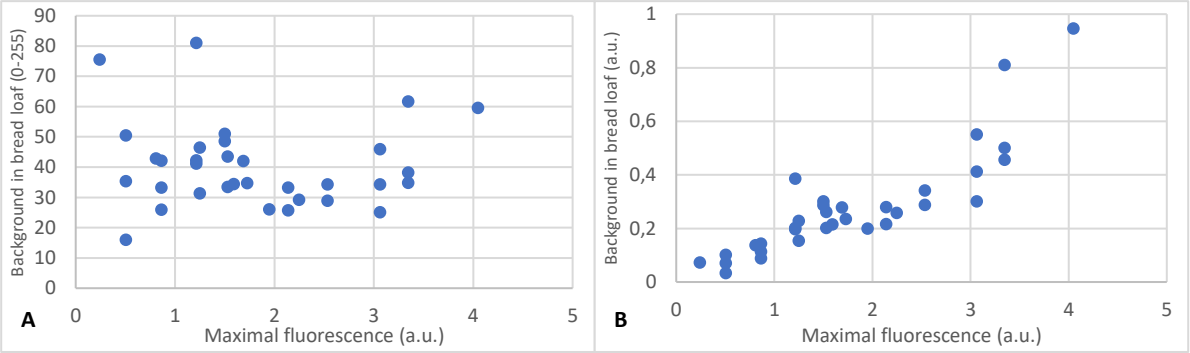

***Figure 12** –Background fluorescence intensity in the bread loaf versus maximal fluorescence intensity*

Figure (A) shows the background fluorescence intensity in the bread loaf in units between 0 and 255. Figure (B) shows the background fluorescence intensity in arbitrary units.

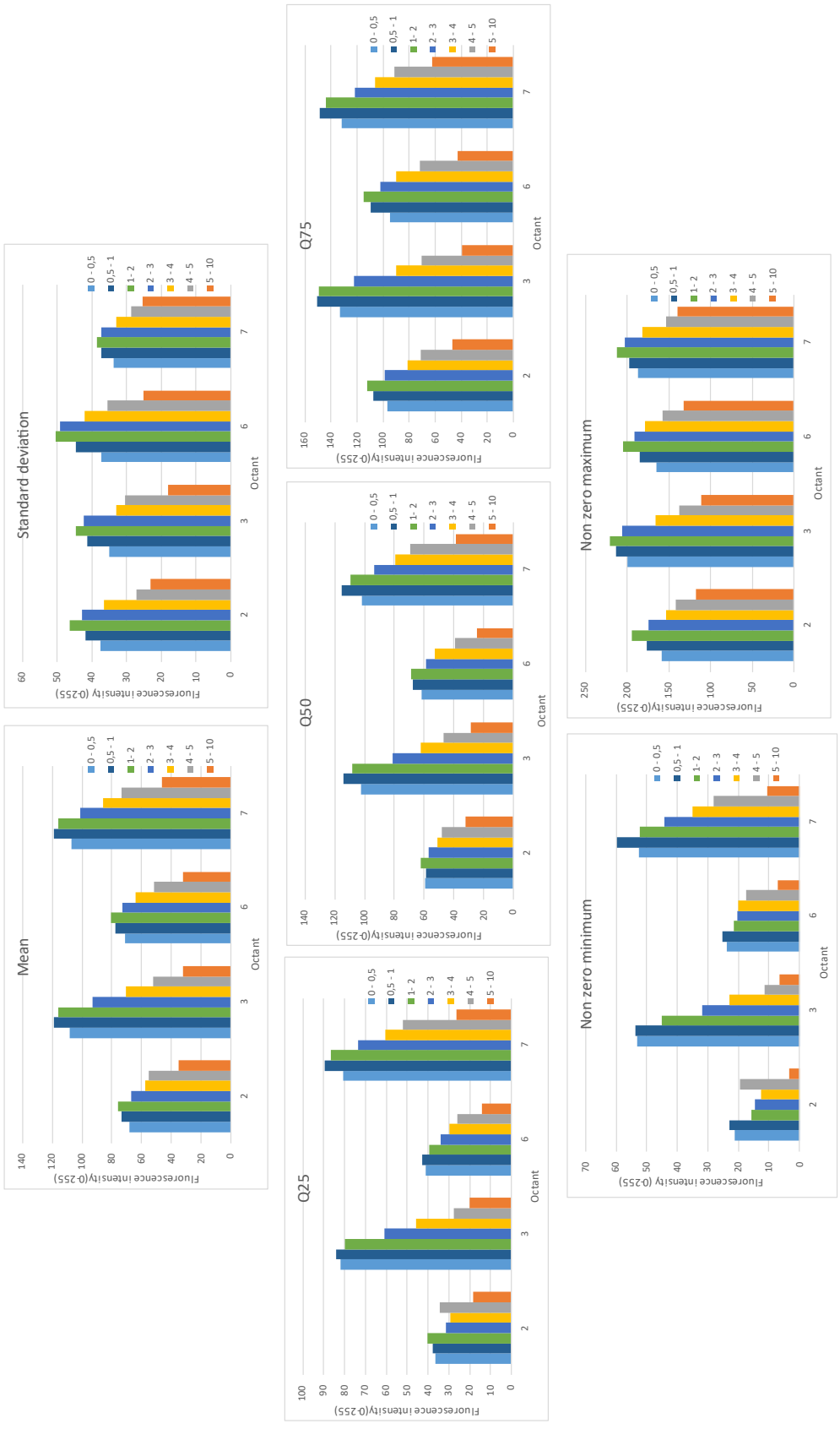

***Figure 13** - Results of the histogram parameters for the different fluorescent halos of the group including all bread loaves*

Effect of preoperative chemotherapy on the peritumoral fluorescent rim

General parameters

The characteristics of the groups with patients receiving preoperative chemotherapy and patients who did not receive chemotherapy can be found in *Table 10.* Five of the seven patients received preoperative chemotherapy, with a total of 21 bread loaves. Twelve bread loaves were analyzed in the non-chemotherapy group. Similar percentages of capsular lesions were found in both groups (57,1% vs 58,3%). The mean size of the tumors, the mean background fluorescence intensity in the tumor, and the mean background fluorescence intensity in the bread loaf were similar for both groups. The largest difference between the two groups was the mean of the maximal fluorescence intensity. The mean maximal fluorescence in the chemotherapy group was 1,29 +/- 0,64 a.u. which was significant lower (P-value <0.001) compared to the non-chemotherapy group (2,68 +/- 0,82 a.u.).

Table 10 *- Characteristics of the preoperative chemotherapy and the non-chemotherapy groups*

Parameter	Chemo (N = 21)	Min - Max	Non-chemo (N = 12)	Min - Max	P-value
Different patients	5	-	2	-	-
Size tumor (cm^2)	2,12 +/- 3,03	0,02 - 11,18	2,70 +/- 1,45	0,63 - 5,86	0.551
Maximal fluorescence (a.u.)	1,29 +/- 0,64	0,24 - 2,54	2,68 +/- 0,82	1,53 – 4,05	<0.001
Capsular tumors	N = 12	-	N = 7	-	-
Background in tumor (0-255)	23,41 +/- 27,64	2,33 – 122,35	21,15 +/- 18,69	3,83 – 68,44	0.809
Background in bread loaves (0-255)	40,77 +/- 14,97	15,93 – 80,94	39,05 +/- 11,19	24,99 – 61,62	0.739

Background fluorescence intensity in the tumor versus maximal fluorescence intensity

The difference in maximal fluorescence intensity between both groups was visible in the comparison between the background fluorescence intensity in the tumor and the maximal fluorescence intensity (*Figure 14*). No difference in background fluorescence intensity in the tumor between both groups was visible. The two groups could be separated with the use of these two parameters, with some overlap in the middle of the graph, based solely on the maximal fluorescence intensity. The use of arbitrary units as units for the mean background fluorescence intensity in the tumor did not change the difference between both groups.

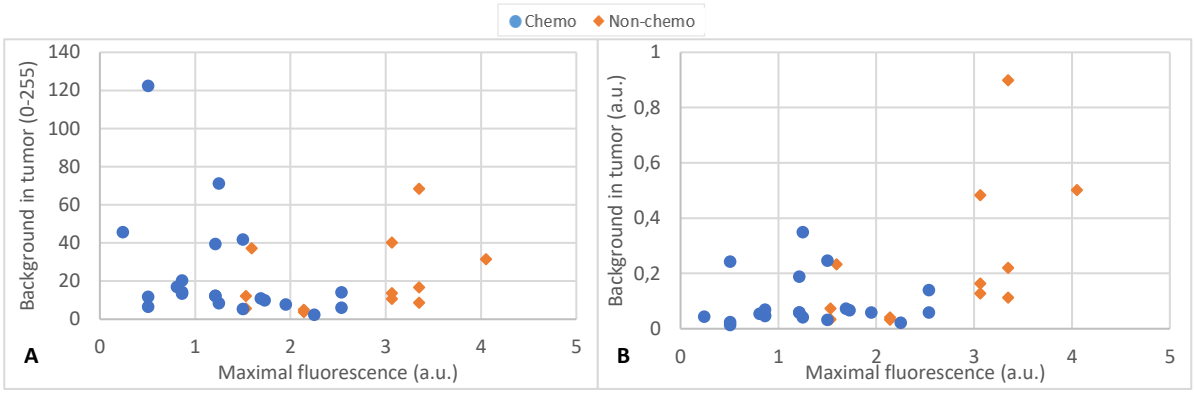

Figure 14 *- Background fluorescence intensity in the tumor versus maximal fluorescence intensity*

Figure (A) shows the background fluorescence intensity in the tumor in units between 0 and 255. Figure (B) shows the background fluorescence intensity in arbitrary units.

Background fluorescence intensity in the tumor versus background fluorescence intensity in the bread loaf

No difference between the chemotherapy and non-chemotherapy groups was seen when comparing background fluorescence intensity in the tumor and the bread loaf (0-255) (*Figure 15*). Similar percentages of datapoints which laid outside of this cluster were found for both groups (29% and 33%).

Background fluorescence intensity in the bread loaf versus maximal fluorescence intensity

No additional differences were found in the comparison of the background fluorescence intensity (for values between 0-255 and in a.u.) and the maximal fluorescence intensity between the chemotherapy and the non-chemotherapy group (*Figure 16*).

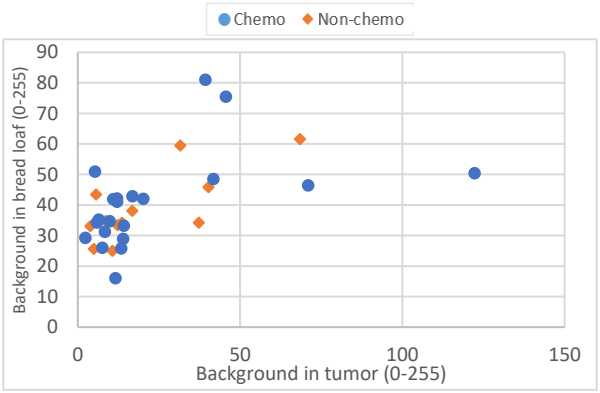

Figure 15 *- Background fluorescence intensity in the bread loaf versus background fluorescence intensity in the tumor*

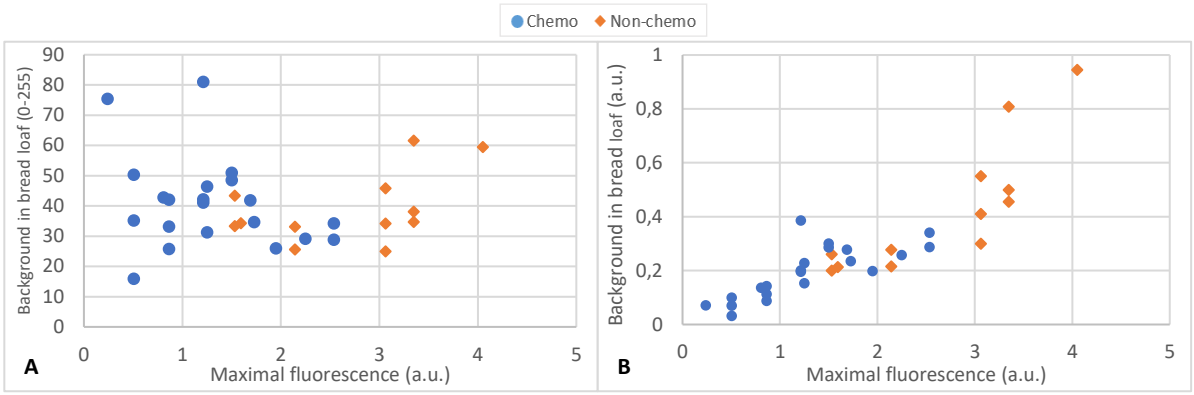

Figure 16 *- Background fluorescence intensity in the bread loaf versus maximal fluorescence intensity*

Figure (A) shows the background fluorescence intensity in the bread loaf in units between 0 and 255. Figure (B) shows the background fluorescence intensity in arbitrary units.

Analysis of the histogram parameters per halo per octant

The results of the histogram parameters for the different octants for the different halos can be found in *Appendix A and Appendix B.* The preoperative chemotherapy group showed higher parameter values in octant 3 and 7, compared to octant 2 and 6, up to the halo of 3 to 4 millimeters, except for the parameter 'standard deviation', which was similar to the analysis of the group including all bread loaves. For both octants 3 and 7 the parameter values of the parameters 'mean', 'Q25', 'Q50', and 'Q75' did increase up to the halo of 0,5 to 1 millimeter from the tumor and then decreased. The parameter 'standard deviation' increased up to the halo of 1 to 2 millimeters from the tumor for both octants. The parameter 'non-zero minimum' increased up to the halo of 0,5 to 1 millimeter from the tumor in octant 7 and only decreased in octant 3. Octants 2 and 6 showed the same distribution of parameter values as found in the analysis of the group including all bread loaves for both octants. All histogram parameter values in octants 2 and 6 increased up to the halo of 1 to 2 millimeters from the tumor after which they decreased. The parameter 'non-zero minimum' in both octants and the parameter 'Q25' in octant 6 were the only parameters that followed a different distribution by decreasing before the halo of 1 to 2 millimeters from the tumor.

Furthermore, octants 3 and 7 showed the highest values for all parameters in the non-chemotherapy group except for the parameter 'non-zero maximum'. The parameter 'non-zero maximum' showed similar values for all four octants. The distribution of the parameter values in octants 3 and 7 was slightly different in the non-chemotherapy group compared to the chemotherapy group. Most parameters increased up to the halo of 1 to 2 millimeters from the tumor. The parameters in octants 2 and 6 followed the same distribution of values of the parameters as seen in the chemotherapy group. The differences between octants 2 and 6 (the octants at the capsule side of the bread loaf) and octants 3 and 7 (octants positioned deeper in the bread loaf) were larger in the non-chemotherapy group compared to the chemotherapy group (*Figure 17*). The non-chemotherapy group showed slightly higher 'mean' fluorescence intensities in octants 3 and 7 compared to the chemotherapy group e.g., the difference in 'mean' (0-255) in the halo of 0,5 to 1 millimeter from the tumor in octant 3 was 21,6 (P-values of 0.296). Octants 2 and 6 showed significantly higher 'mean' values in the non-chemotherapy group e.g., the difference in 'mean' (0-255) in the halo of 0,5 to 1 millimeter from the tumor in octant 2 was 47,4 (P-values of 0.007).

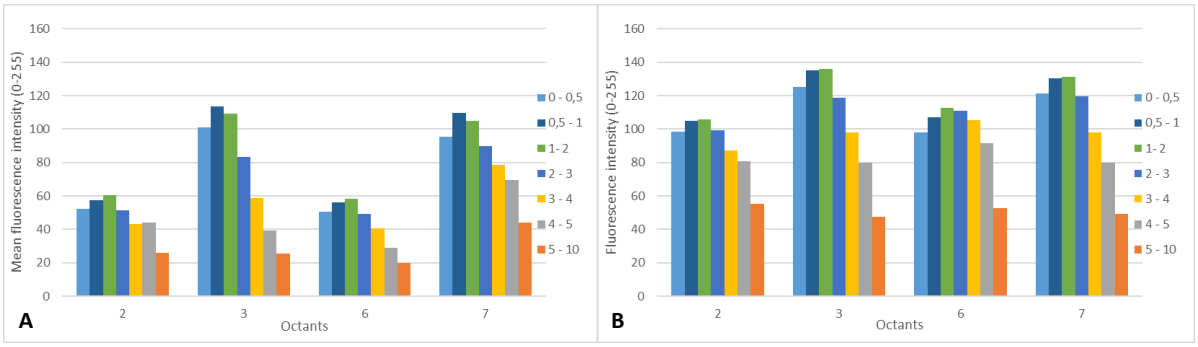

Figure 17 *- Histogram parameter 'mean' values per halo per octant of the preoperative chemotherapy and non-chemotherapy groups*

Figure (A) shows the mean 'mean' values of the preoperative chemotherapy group. Figure (B) shows the mean 'mean' values of the non-chemotherapy group.

Effect of the location of the CRLM in the liver on the peritumoral fluorescent rim

General parameters

The characteristics of the groups containing capsular lesions and subcapsular lesions can be found in *Table 11.* Four bread loaves were not divided into the groups with capsular or subcapsular lesions as they were too damaged to be identified as a capsular or a subcapsular lesion. The groups of capsular and subcapsular lesions showed a comparable mean of the size of the tumors and background fluorescence intensity in the bread loaves. The group with capsular lesions had a marginally higher rate of patients receiving preoperative chemotherapy (63,2% vs 50%). Furthermore, the capsular lesion group showed a higher mean maximal fluorescence intensity (P-value of 0.175) and mean background fluorescence intensity in the tumor (P-value of 0.249). Both parameters showed a higher spread in values in the group with capsular lesions.

Table 11 *- Characteristics of the capsular and subcapsular lesions groups*

Parameter	Capsular (N = 19)	Min - Max	Subcapsular (N = 10)	Min - Max	P-value
Different patients	N = 5	-	N = 3	-	-
Size tumor (cm^2)	2,67 +/- 2,98	0,31 – 11,18	2,59 +/- 1,70	0,44 - 5,86	0.944
Maximal fluorescence intensity (a.u.)	2,15 +/- 1,02	0,81 - 4,05	1,66 +/- 0,43	1,21 - 2,54	0.175
Preoperative chemotherapy	N = 12	-	N = 5	-	-
Background in tumor (0-255)	22,13 +/- 19,28	2,33 - 71,05	13,88 +/- 12,60	3,82 - 39,36	0.249
Background in bread loaves (0-255)	38,37 +/- 10,37	24,99 - 61,62	41,90 +/- 14,63	25,63 - 80,94	0.474

Background fluorescence intensity in the tumor vs maximal fluorescence intensity

Both the capsular and subcapsular lesions groups showed no correlation between the background fluorescence intensity in values between 0-255 in the tumor and the maximal fluorescence intensity (*Figure 18A*). The subcapsular group clustered between 0 and 40 for the background fluorescence intensity in the tumor and between 1 and 2,5 a.u. for the maximal fluorescence intensity. The group with capsular lesions did not cluster. Both types of lesions could not be separated using these two parameters. Furthermore, the background fluorescence intensity in the tumor in a.u. and the maximal fluorescence intensity did not show a correlation (*Figure 18B*). However, the datapoints of the subcapsular lesions showed clustering.

Background fluorescence intensity in the tumor versus background fluorescence intensity in the bread loaf

The comparison between background fluorescence intensity in the tumor and bread loaf can be found in *Figure 19*. Both types of lesions showed datapoints inside and outside of the cluster. The capsular lesions group showed the most outliers (42,1% (8/19) versus 20% (2/10)).

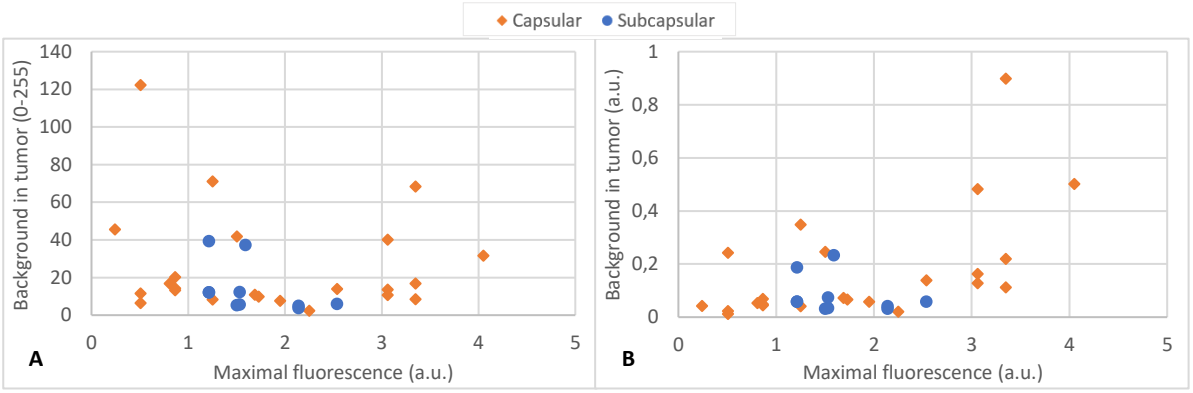

***Figure 18** - Background fluorescence intensity in the tumor versus maximal fluorescence intensity*

Figure (A) shows the background fluorescence intensity in the tumor in units between 0 and 255. Figure (B) shows the background fluorescence intensity in arbitrary units.

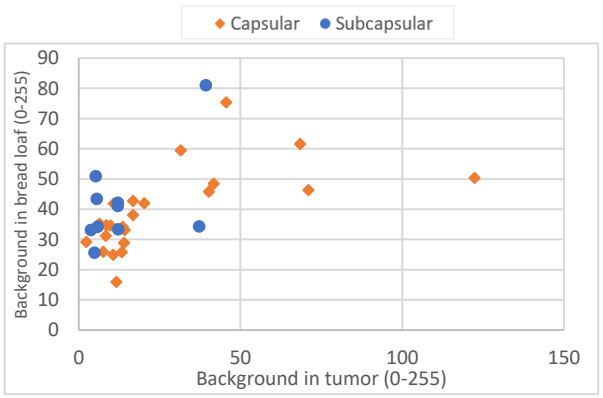

***Figure 19** - Background fluorescence intensity in the tumor versus in the bread loaf*

Background fluorescence intensity in the bread loaf versus maximal fluorescence intensity

No additional differences between both types of lesions were found by comparing the background fluorescence intensity (for values between 0-255 and in a.u.) in the bread loaf and the maximal fluorescence intensity (*Figure 20*).

Analysis of the histogram parameters per halo per octant

The results of the histogram parameters for the different octants for the different halos can be found in *Appendix C and Appendix D*. The highest mean values for the parameters 'mean', 'Q25', 'Q50', 'Q75', 'non-zero minimum', and 'non-zero maximum' were found in octants 3 and 7 for the capsular lesions. The parameter values in these octants increased up to the halo of 0,5 to 1 millimeter from the tumor and then decreased over a steep line. This was comparable to the distribution of the parameter values for the group including all bread loaves. The only exception was the 'non-zero maximum' in octant 7, which increased up to the halo of 1 to 2 millimeters from the tumor. The same distribution of values was seen for octants 2 and 6. However, both octants showed lower parameter values compared with octants 3 and 7 and both octants showed more parameters with a slightly different distribution of values as more parameters showed an increase up to the halo of 1 to 2 millimeters from the tumor (*Figure 21A & Figure 22A*).

In the subcapsular group, the highest 'mean' values were found in octants 2 and 6. Octants 3 and 7 show slightly lower 'mean' values for every halo. This was different from the capsular group as the capsular group showed higher 'mean' values in octants 3 and 7. However, the largest difference in the middle four octants between the subcapsular and capsular groups was the distribution of values of the parameters. All parameter values, except for the 'non-zero minimum' in octant 2 and 7, increased in the subcapsular group to a minimum of the halo of 1 to 2 millimeters from the tumor before decreasing. The 'mean' value increased up to the halo of 2 to 3 millimeters from the tumor in octants 2, 3, and 6, before decreasing. The 'mean' in octant 7 increased up to the halo of 3 to 4 millimeters from the tumor (Figure 21*B*).

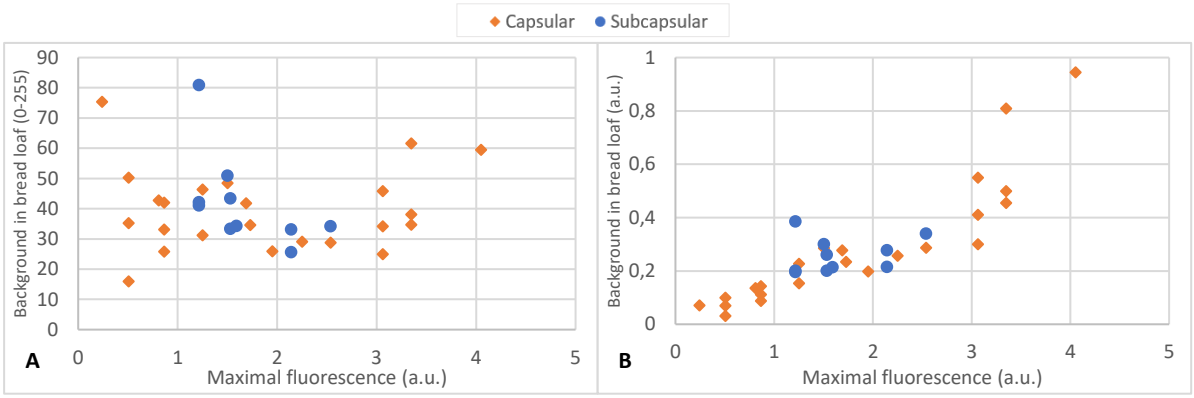

Figure 20 *- Background fluorescence intensity in the bread loaf versus maximal fluorescence intensity*

Figure (A) shows the background fluorescence intensity in the bread loaf in units between 0 and 255. Figure (B) shows the background fluorescence intensity in arbitrary units.

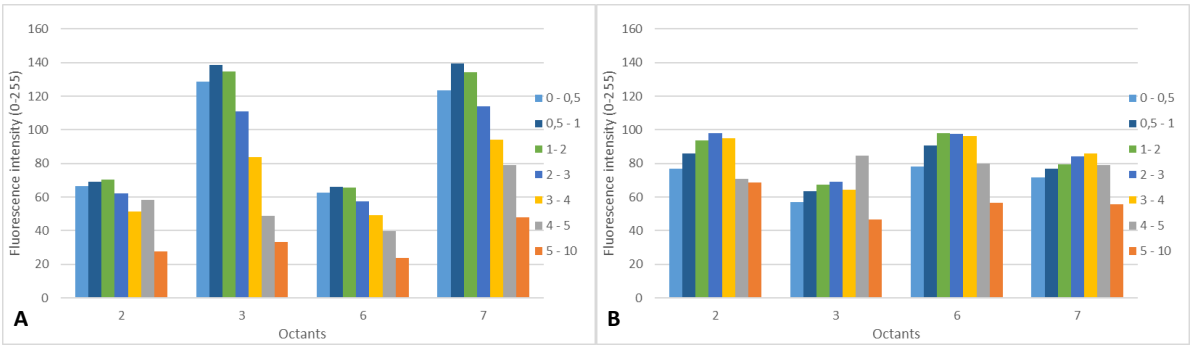

Figure 21 *- Histogram parameter 'mean' values per halo per octant of the capsular lesions and subcapsular lesions groups*

Figure (A) shows the mean 'mean' values of the capsular lesions group. Figure (B) shows the mean 'mean' values of the subcapsular lesions group.

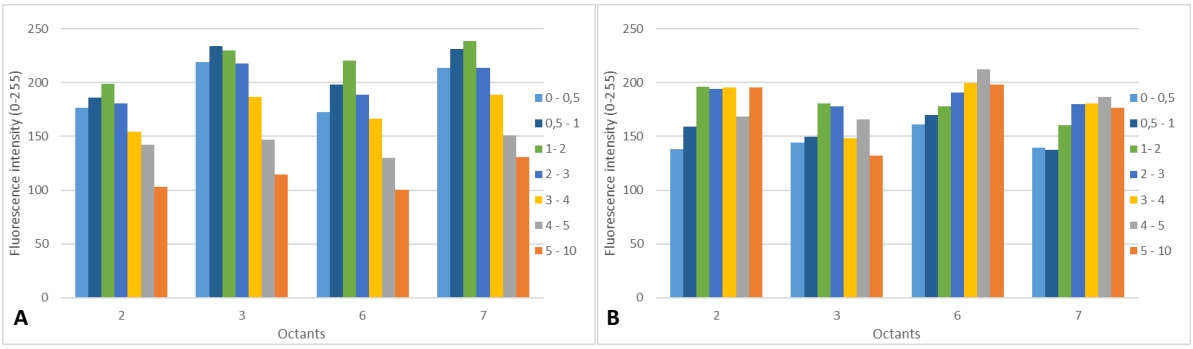

Figure 22 *- Histogram parameter 'non-zero maximum' values per halo per octant of the capsular lesions and subcapsular lesions groups*

Figure (A) shows the mean 'mean' values of the capsular lesions group. Figure (B) shows the mean 'mean' values of the subcapsular lesions group.

Effect of the size of the CRLM on the peritumoral fluorescent rim

General parameters

The bread loaves were divided into four different groups to analyze the effect of the size of the tumor on the peritumoral rim. Groups with tumors smaller than 1 cm^2 (N = 14), with tumors from 1 to 2 cm^2 (N = 5), with tumors from 2 to 3 cm^2 (N = 6), and with tumors larger than 3 cm^2 (N = 9) were separated. The characteristics of these groups can be found in *Table 12* and *Table 13*. The groups were difficult to compare as the patient and tumor-specific variables differed much between the four groups. A clear trend was observed in the mean background fluorescence intensity in the tumor. The mean background fluorescence intensities decreased when the tumor size increased.

Table 12 *- Characteristics of the groups with tumors from 0 to 1 cm^2 and 1 to 2 cm^2*

Parameter	**0-1 cm^2 (N = 14)**	**Min - Max**	**1-2 cm^2 (N = 5)**	**Min - Max**
Different patients	N = 4	-	N = 4	-
Size tumor (cm^2)	0,40 +/- 0,24	0,02 – 0,79	1,39 +/- 0,26	1,00 – 1,64
Maximal fluorescence (a.u.)	1,41 +/- 0,81	0,24 – 3,35	2,35 +/- 0,83	1,21 – 3,35
Preoperative chemotherapy	N = 13	-	N = 2	-
Capsular tumors	N = 8	-	N = 2	-
Background in tumor (0-255)	33,15 +/- 32,31	6,46 – 122,35	22,46 +/- 13,76	5,89 – 40,21
Background in bread loaves (0-255)	43,69 +/- 17,77	15,93 – 80,94	38,68 +/- 4,39	34,21 – 45,82

Table 13 *- Characteristics of the groups with tumors from 2 to 3 cm^2 and tumors larger than 3 cm^2*

Parameter	**2-3 cm^2 (N = 6)**	**Min - Max**	**3+ cm^2 (N = 8)**	**Min - Max**
Different patients	N = 2	-	N = 3	-
Size tumor (cm^2)	2,61 +/- 0,30	2,08 – 2,92	6,08 +/- 2,48	3,01 – 11,18
Maximal fluorescence (a.u.)	2,75 +/- 0,95	1,50 – 4,05	1,87 +/- 0,27	1,53 – 2,25
Preoperative chemotherapy	N = 2	-	N = 4	-
Capsular tumors	N = 5	-	N = 4	-
Background in tumor (0-255)	18,60 +/- 13,35	5,36 – 41,79	7,16 +/- 3,34	2,33 – 12,26
Background in bread loaves (0-255)	42,13 +/- 11,76	24,99 – 59,48	33,38 +/- 6,02	25,63 – 43,40

Background fluorescence intensity in the tumor versus maximal fluorescence intensity

The comparison between the background fluorescence intensity and the maximal fluorescence intensity can be found in *Figure 23*. The comparison between the background fluorescence intensity in the tumor in units between 0 and 255 and the maximal fluorescence intensity showed tumors between 1 and 3 cm^2 did not cluster. However, all datapoints of tumors for the group with tumors of 3+ cm^2 did cluster between maximal fluorescence intensities of 1,5 to 2,3 a.u. and between background fluorescence intensities in the tumor of 0 to 20 (0-255). However, these datapoints could not be separated from the other groups as one datapoint from the group with tumors between 2 and 3 cm^2 was present in this cluster. Most of the datapoints from tumors smaller than 1 cm^2 did cluster as most of the bread loaves showed low maximal fluorescence intensities. However, this group of tumors showed 2 outliers with maximal fluorescence intensities of 2,5 and 3,3 a.u. The use of arbitrary units for the background fluorescence intensity in the tumors did not add additional information (*Figure 23B*).

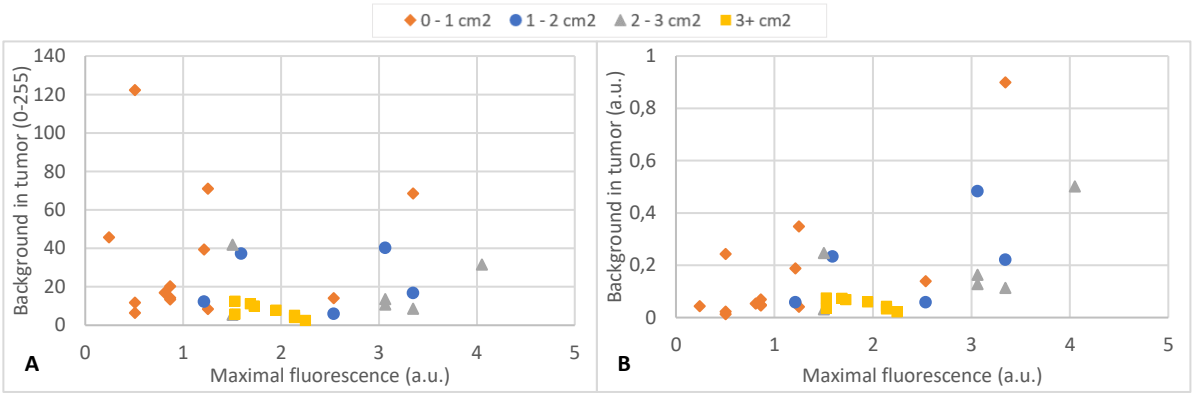

Figure 23 *- Background fluorescence intensity in the tumor versus maximal fluorescence intensity*

Figure (A) shows the background fluorescence intensity in the tumor in units between 0 and 255. Figure (B) shows the background fluorescence intensity in arbitrary units.

Background fluorescence intensity in the tumor versus background fluorescence intensity in the bread loaf

Datapoints from all 4 different sized tumor groups laid in the cluster, which is described in the analysis of the group including all bread loaves. The group with tumors larger than 3 cm^2 did not present outliers of this cluster (0/8). The groups with tumors smaller than 1 cm^2, between 1 and 2 cm^2, and between 2 and 3 cm^2 showed 42,9% (6/14), 40% (2/5), and 33,3% (2/6) outliers, respectively.

Background fluorescence intensity in the bread loaf versus maximal fluorescence intensity

The comparison of the background fluorescence intensity in the bread loaves in units between 0 and 255 with the maximal fluorescence intensity displayed similar results to the comparison of the maximal fluorescence intensity and the background fluorescence intensity in the tumor (*Figure 25A*). The groups with the smallest and largest tumors clustered and the groups with tumors between 1 and 3 cm^2 showed a larger spread of datapoints and did therefore not cluster. The dimensions of the clusters of the groups of the tumors smaller than 1 cm^2 and larger than 3 cm^2 decreased when the background fluorescence intensity in the bread loaf was measured in arbitrary units (*Figure 25B*). However, overlap with datapoints from other groups increased. Especially the cluster of the tumors larger than 3 cm^2 showed more overlap as three datapoints of the groups between 1 and 3 cm^2 were positioned in the cluster. Therefore, the groups were more difficult to distinguish with the use of arbitrary units.

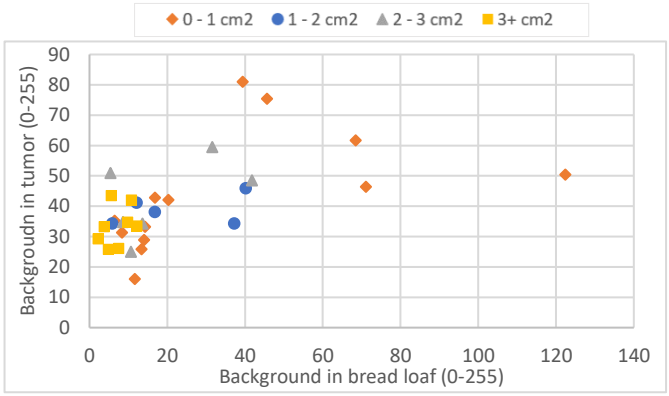

Figure 24 *- Background fluorescence intensity in the tumor versus background fluorescence intensity in the bread loaf*

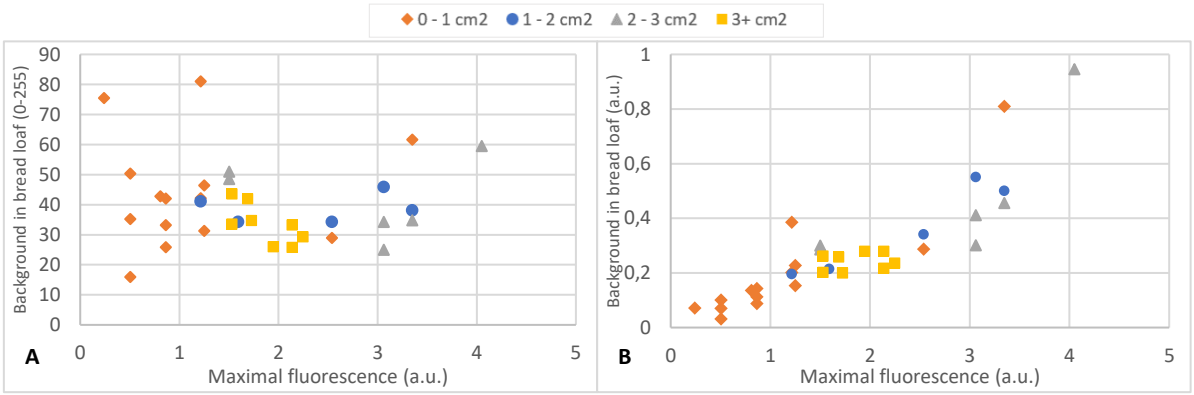

Figure 25 *- Background fluorescence intensity in the bread loaf versus maximal fluorescence intensity*

Figure (A) shows the background fluorescence intensity in the bread loaf in units between 0 and 255. Figure (B) shows the background fluorescence intensity in arbitrary units.

Analysis of the histogram parameters per halo per octant

The results of the histogram parameters for the different octants for the different halos can be found in *Appendix E, Appendix F, Appendix G, and Appendix H.* The group with tumors smaller than 1 cm^2 showed the highest parameter values in octants 3 and 7. The parameter values were all significantly higher up to the halo of 4 to 5 millimeters compared to octants 2 and 6 e.g., the difference in 'mean' (0-255) in the halo of 0,5 to 1 millimeter from the tumor between octant 2 and was 79,7 (P-values < 0.001) The peak in mean 'mean' values in octant 2 of the smallest tumors was 56,0 which was significantly lower compared to the 135,3 in octant 3. Octants 6 and 7 showed similar results (59,5 and 116,1) (*Figure 26A*). The parameter values, except for the 'non-zero maximum' and the 'standard deviation', in octants 3 and 7 increase up to the halo of 0,5 to 1 millimeter from the tumor after which they decreased. Octant 6 showed an increase up to the halo of 1 to 2 millimeters from the tumor. Octant 2 displayed the same distribution of parameter values as octant 6. However, especially at the halo of 4 to 5 millimeters from the tumor, the distribution was disturbed by an increase in all parameter values compared to the halo of 3 to 4 millimeters from the tumor. Moreover, the parameter 'mean' showed values for octant 2, 3, and 6 in the halo of 5 to 10 millimeters from the tumor of 17,1, 29,8, and 22,6, respectively. These values were considerably lower than the mean background fluorescence intensity in the bread loaves which was 43,69 +/- 17,77 for the smallest tumors.

The group with tumors between 1 and 2 cm^2 presented comparable results to the group with tumors smaller than 1 cm^2. The highest parameter values were found in octants 3 and 7 except for the parameters 'non-zero maximum' and 'standard deviation'. However, the difference between the octants 3 and 7 compared to octants 2 and 6 was smaller in the group with tumors between 1 and 2 cm^2. The parameter values of octants 3 and 7 increased up to the halo of 0,5 to 1 millimeter from the tumor and the parameter values of octant 2 increased up to the halo of 1 to 2 millimeters from the tumor. However, the parameter values in octant 6, except for the 'non-zero minimum', did increase up to the halo of 2 to 3 millimeters from the tumor. The halo of 5 to 10 millimeters from the tumor of octant 3 was the only halo to show a mean 'mean' value of the halo of 5 to 10 millimeters from the tumor (27,6), which was considerably lower than the mean background fluorescence intensity (38,68 +/- 4,39) of the group with tumors between 1 and 2 cm^2 (*Figure 26B*).

In the group with tumors between 2 and 3 cm^2, octant 6 showed similar values for the parameter 'mean' compared to octant 3 and 7. The distribution of the most parameter values of octant 6 with increasing distance from the tumor was similar to the distribution of parameter values of octants 3 and 7. The values increased up to the halo of 0,5 to 1 millimeter from the tumor for most parameters. Octants 3 and 7 displayed for the tumors between 2 and 3 cm^2 lower 'non-zero minimum' and higher 'non-zero maximum' values in most halos compared to the group of tumors between 1 and 2 cm^2. However, the comparison of the group with tumors of the 2 to 3 cm^2 with the group with tumors smaller than 1 cm^2 did not show differences.

The group with tumors larger than 3 cm^2 presented more comparable octants. The mean 'mean' for every halo was comparable for octants 2, 3, and 7. Octant 6 showed slightly lower values. However, the difference between the octants was smaller compared to the difference in octants in the other groups. Octant 7 showed an increase in most parameter values up to the halo of 0,5 to 1 millimeter from the tumor. Octant 6 showed an increase up to the halo of 1 to 2 millimeters from the tumor as seen in the other groups with different sized tumors. However, octant 2

showed an increase up to the halo of 2 to 3 millimeters from the tumor and octant 3 up to the halo of 1 to 2 millimeters from the tumor for most parameter values. This was one millimeter farther away from the tumor compared to the groups with smaller tumors (*Figure 26D*).

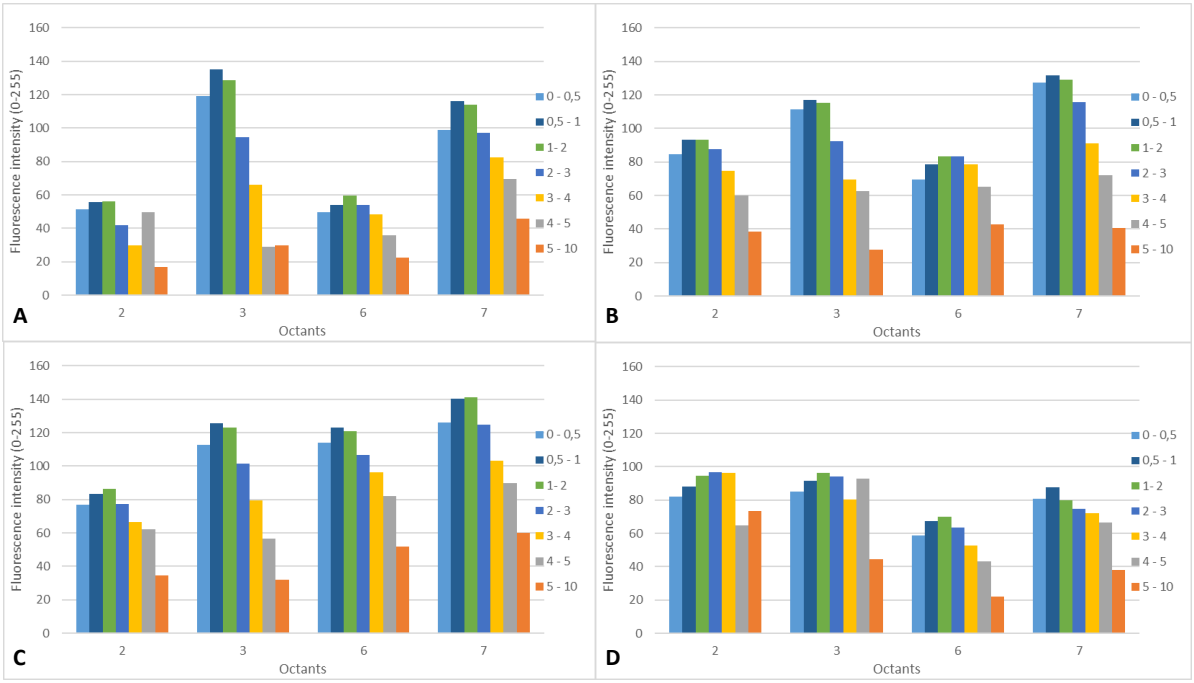

Figure 26 *- Histogram parameter 'mean' values per halo per octant of the groups with different sized tumors*

Figure (A), (B), (C), and (D) show the mean 'mean' values of the groups with tumors of the size 0-1 cm², 1-2 cm², 2-3 cm², and 3+ cm², respectively.

Propagation of fluorescence through tissue

Equation 2 was applied on the data from the parameter 'mean' of octant 3 of the group including all bread loaves, the group with patients who did not receive preoperative chemotherapy, and the group of capsular lesions (*Table 14*). The results are summarized in *Table 15*.

Table 14 *- Values of histogram parameter 'mean' per halo of octant for the group including all bread loaves, the non-chemotherapy group, and the capsular lesions group*

	Octant 3 All bread loaves	*Octant 3 Non-chemotherapy*	*Octant 3 Capsular lesions*
Distance of halo borders to tumor (mm)	**Mean fluorescence intensity**	**Mean fluorescence intensity**	**Mean fluorescence intensity**
0 – 0,5	108,41	125,29	128,46
0,5 – 1	118,77	135,22	138,60
1 – 2	115,78	135,86	134,54
2 – 3	93,21	118,68	110,99
3 – 4	70,52	98,02	83,88
4 – 5	52,20	79,70	48,98
5 - 10	32,13	47,40	33,08

Table 15 *- Results of the expected measured fluorescence intensities of octant 3 for the group including all bread loaves, the non-chemotherapy group, and the capsular lesions group*

	All bread loaves		**Non-chemotherapy**		**Capsular lesions**	
Distance to tumor (mm)	**Expected measured intensity**	**Percentage of maximal fluorescence intensity**	**Expected measured intensity**	**Percentage of maximal fluorescence intensity**	**Expected measured intensity**	**Percentage of maximal fluorescence intensity**
0,5	52,23	20,48%	60,37	23,68%	61,89	24,27%
1	105,74	41,47%	121,22	47,54%	124,26	48,73%
2	198,71	77,92%	230,70	90,47%	232,10	91,02%
3	257,92	101,14%	309,16	121,24%	303,23	118,92%
4	287,91	112,91%	357,64	140,25%	339,40	133,10%
5	296,76	116,38%	382,43	149,97%	338,17	132,62%
10	252,51	99,03%	346,09	135,72%	275,54	108,06%

The tipping point for the group including all bread loaves, when using *Equation 2*, laid between 5 and 10 millimeters from the tumor. Thus, it is expected that the fluorescence intensity will increase when moving towards the tumor when imaging during surgery. At a certain point between 10 and 5 millimeters from the tumor, the fluorescence intensity is then expected to decrease. The group with patients who did not receive preoperative chemotherapy showed the same distribution of expected fluorescence intensity values. However, when the lesion was capsular, the measured fluorescence intensity displayed an increase until 4 millimeters from the tumor.

Discussion

To calculate the interobserver error, 10 bread were delineated by a pathologist and a researcher. The calculation of the Sørensen-Dice coefficient showed eight pairs of delineations with a coefficient higher than 0.9. Three of these eight pairs of delineations showed coefficients of 0.95 or higher. However, two pairs of delineations showed low coefficients (0.566 and 0.797). Manual inspection and evaluation of the delineations by the pathologist showed a tumor that was difficult to delineate and a tumor in which the researcher potentially missed tumor tissue. Therefore, the delineation of CRLM based on images generated with the PEARL imaging system proved to be difficult in 20% of the delineations. However, the operation was reliable in 80% of the delineations. The delineations of the pathologist were not considered the 'ground truth' as the pathologist delineated CRLM in images generated by the PEARL imaging system. Therefore, the Sørensen-Dice coefficient did not indicate the accuracy of the researcher. However, the high coefficients suggest the delineation of CRLM based on the PEARL images was an operation that was reproducible between different observers.

The lack of a 'ground truth' is a problem that must be solved to be able to precisely predict resection margins with the use of fluorescence intensity. However, regarding this research, the similarities between the delineations of the researcher and the pathologists were assumed to be sufficient to be able to do calculations on the peritumoral fluorescent rim.

The current gold standard in the determination of the resection margin is histological research. However, the standard protocol of histological research does not include the enclosure and examination of the whole tumor. To generate ground truth images, the enclosure and examination of the whole resected tumor are needed to validate the delineations. Therefore, a new excision and processing protocol must be developed to be used at the Department of Pathology.

For the main part of this research, all 33 bread loaves were used. Before data was generated out of the bread loaves, all bread loaves were divided into octants to gain more knowledge about the distribution of ICG around the CRLM. However, octants 1, 4, 5, and 8, did not contain enough data to be able to make a representative analysis in most of the tumors. This was due to two factors. The first factor is that only data in the bread loaves was used to generate data. The areas, which did not contain liver or tumor tissue, were filtered out.

When a tumor was resected with a small resection margin, the halos which were situated farther away from the tumor could not have overlap with the bread loaf (*Figure 27*). Besides, one centimeter was added from the edge of the bread loaf in the horizontal and vertical direction to create the octants. In case the tumor was small, octants 1, 4, 5, and 8 would also not contain information. A visualization of this problem can be found in *Figure 28*.

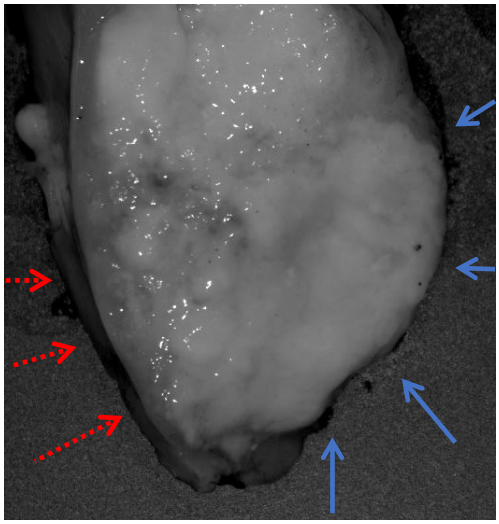

Figure 27 *- Image of a resected tumor with a small resection margin*

This figure shows a tumor with a small resection margin. When going farther away from the tumor the chance rises that the halo will not contain data as there will be no overlap with the bread loaf. In this image there is practically no liver tissue left (blue uninterrupted arrows). However, there are also parts (red dotted arrows) were there is a chance the halos farther away will not contain data.

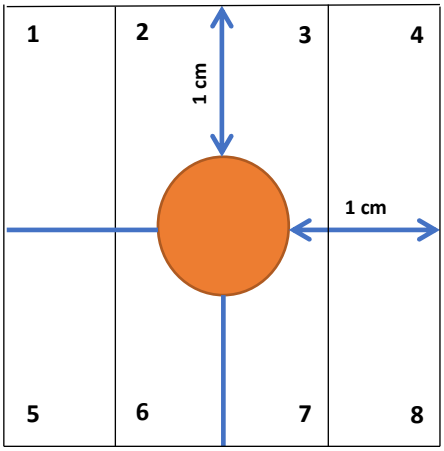

Figure 28 *- Visualization of the problem of octants which do not contain data caused by a small tumor*

The orange circle visualizes a small tumor. The vertical and horizontal lines visualize the edges of the octants. As displayed, the octants at the outside will not contain data for the first few halos.

Moreover, the use of data only present in bread loaves influenced the data of the middle four octants (*Figure 27*). A small resection margin increased the chance for the varying halos to fall outside of the bread loaf. This resulted in 'mean' values of zero. Besides, the border of the tumor did provide pixel intensity values of zero. This was caused by for example the effect of cauterization, ink, or a small error that was made during the delineation of the bread loaf. *Figure 29* shows the effect of ink and cauterization on the fluorescence intensity.

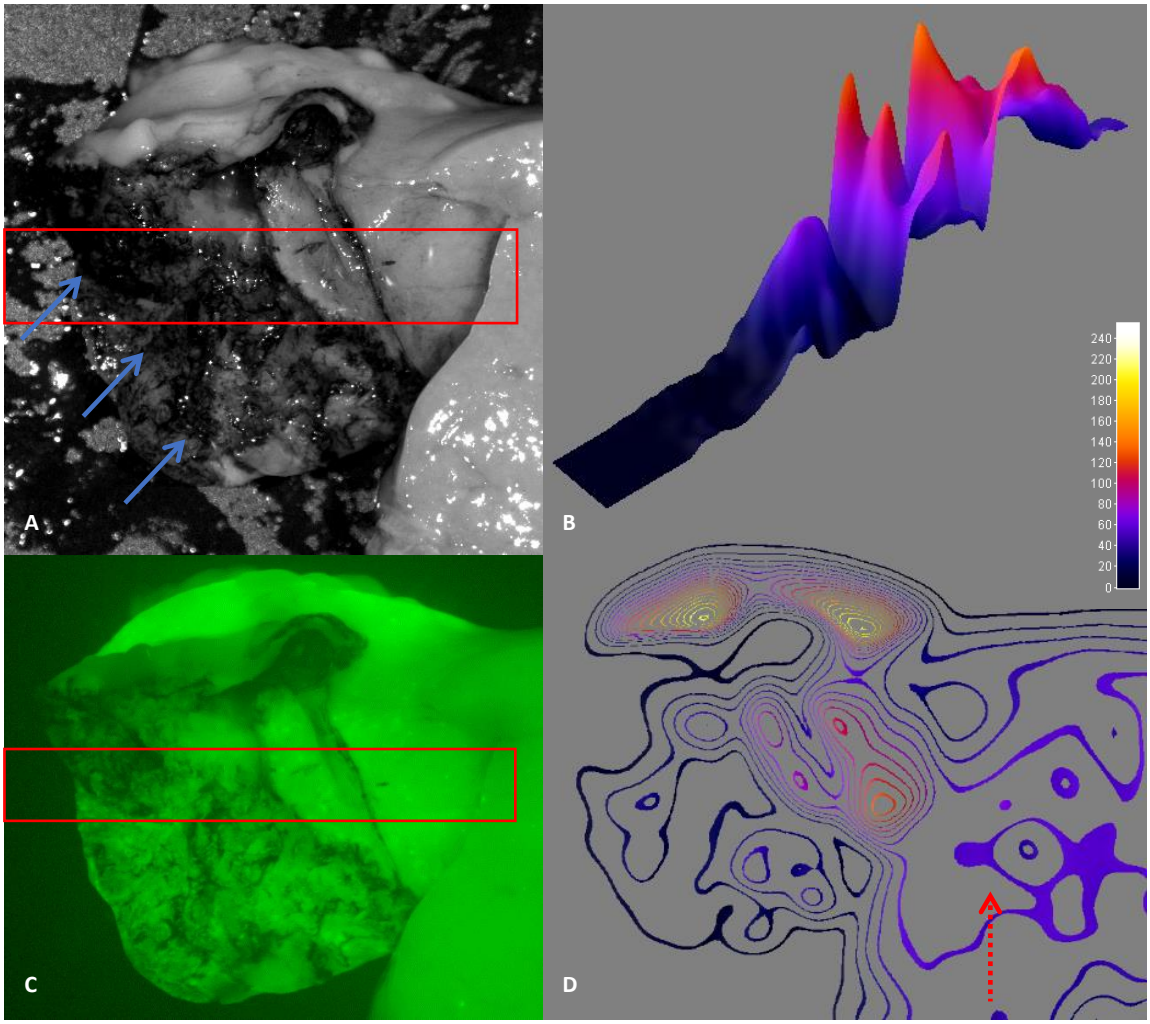

Figure 29 *- Effect of cauterization and ink on measured fluorescence intensity with the PEARL imaging system*

(A) shows a black and white image made with the PEARL. The ink, applied before imaging, is clearly visible (blue undisrupted arrows). (B) shows a graph of the fluorescence intensities from the box in (A) and (C). The left side of the image is the left side in (A) and (C). (C) shows a boosted fluorescent image made with the PEARL. Dark spots (low fluorescence intensity) are visible where ink is clearly visible in (A). (D) shows a fluorescent heatmap of the bread loaf. Low fluorescent intensities are found in the section where ink is applied on the tumor. These regions show lower fluorescent intensities compared to the fluorescent intensities in liver tissue (red dotted arrow). High fluorescence intensities are seen near these regions. There is no ink applied on the high fluorescent regions.

A pixel with the value zero that was only included in one of the two halos, which were subtracted from each other, resulted in a pixel value of one in the subtracted halo. A whole halo only consisting of the background value minus one, which was not used in the calculations of the histogram parameters, and this value one resulted in the values zero or one for the histogram parameters 'mean', 'Q25', 'Q50', 'Q75', 'Non-zero minimum', 'non-zero maximum' and 'standard deviation'. The mean histogram parameter values per halo of all bread loaves were therefore, in most of the cases, an underestimation of their real values. *Table 16* shows the mean 'mean' values in the different subtracted halos for octants 2 and 3 of the group including all bread loaves, after deleting the ones and zeros from the group.

***Table 16** - Corrected mean values per halo for the histogram parameter 'mean' of octants 2 and 3 with data from the whole group*

Halo border distance to tumor (mm – mm)	Mean 'mean' values of octant 2 (0-255)	Corrected mean 'mean' values of octant 2 (0-255)	Mean 'mean' values of octant 3 (0-255)	Corrected mean 'mean' values of octant 3 (0-255)
0 - 0,5	68,26	68,26	108,41	108,41
0,5 – 1	73,71	73,71	118,77	118,77
1 – 2	75,58	75,58	115,78	115,78
2 - 3	66,92	70,68	93,21	93,21
3 - 4	57,55	64,97	70,52	73,25
4 - 5	55,35	59,79	52,20	59,19
5 - 10	34,99	45,82	32,13	39,23

* mm = millimeter

With increasing distance to the tumor, the effect of the correction becomes visible. The highest decrease was seen in the halo from 5 to 10 millimeters from the tumor in octant 2. The correction showed a decrease of 23,6% of its initial mean 'mean' value. However, this correction only corrected for halos consisting out of only zeros or ones. Halos with higher mean 'mean' values than one could still contain several pixels with intensities of zeros and ones. Therefore, it was assumed that the mean 'mean' values of the halos close to the borders of the bread loaves still showed an underestimation of the real mean 'mean' values per halo. This distortion was likely to be present in all other histogram parameters.

Correction for pixel intensities of zero or one will be difficult as all pixels will have to be checked manually. Real pixel values of zero or one must not be corrected. To be able to analyze large groups with bread loaves, the method must be objective and automatic. Therefore, it is assumed that the method used during this research is the right method to use. However, to be able to obtain complete data, which is not distorted by missing or wrong data, bread loaves with tumors large enough to prevent the situation in *Figure 28* and with enough liver tissue around the tumor to fill all octants, must be analyzed. This must be done to ultimately be able to make a complete and precise prediction of distances to a tumor with the use of the fluorescent rim.

Two other parameters which could be calculated more accurately are the background fluorescence intensity in the bread loaves and in the tumor.

The analysis of the general parameters of the group including all bread loaves showed a high spread in datapoints for the background fluorescence intensity in the tumor and the bread loaf. This could be addressed to the differences in the size of the bread loaves and tumors. The calculation of the background fluorescence intensity in the bread loaf proved to be difficult as the fluorescence in the liver tissue was inhomogeneous and not all bread loaves had enough 'fluorescent halo-free' liver tissue to calculate the background fluorescence intensity in the bread loaf. Therefore, manually selecting an area to calculate the background fluorescent intensity was not achievable. Besides, manually selecting an area would add a subjective factor to the calculations. In this research an automatic and objective method was used to calculate the background fluorescence intensity. The background fluorescence intensity was calculated as the mean fluorescence intensity in the whole bread loaf. Nevertheless, high background fluorescence intensities were measured. These high background fluorescence intensities were especially found in small bread loaves. In small bread loaves the fluorescent halo around the tumor had a significant influence on the background fluorescence intensity. However, the objective and automatic method used during this research is believed to be the superior method to use for especially large groups compared to a manual method. Besides, manually selecting the background fluorescence intensity in the bread loaf will not assure exclusion of high background fluorescence intensities.

A high background fluorescence intensity in the tumor could be a result of the small size of the tumor in the bread loaf. A small tumor could mean that the tumor edge is located in the bread loaf. Therefore, the fluorescent halo behind that edge could provide fluorescence to the measurements. This effect was less observed in larger tumors. The second source of a high background intensity in the tumor in units between 0 and 255 was a low maximal fluorescence intensity in the image of the bread loaf. The different comparisons between the background fluorescence intensity in the tumor, in the bread loaf, and the maximal fluorescence intensity did show this phenomenon (*Figure 10, Figure 11, and Figure 12*). A relatively high amount of data showed high background fluorescence intensities and low maximal fluorescence intensities. The low maximal fluorescence intensity affected the ratio to the background fluorescence intensity. However, a low maximal fluorescence intensity indirectly indicates a halo with low accumulation of ICG around the tumor was found in these bread loaves.

The comparison between both background fluorescence intensities showed that the background fluorescence intensity in both the tumor and bread loaf could be predicted when the maximal fluorescence intensity is retrieved. Most datapoints could be clustered between 0 and 20 for the tumor and 25 and 55 for the bread loaf background fluorescence intensity (0-255). Clustering of the datapoints in the comparison of both fluorescent background intensities suggested that both parameters were related to the maximal fluorescence intensity and each other. When the background fluorescent intensity in the bread loaf is retrieved it is possible to predict the background fluorescent intensity in the tumor and the maximal fluorescence intensity in an acceptable range and vice versa. However, 30,3% of the datapoints (10/33) were not present in this cluster. Most of these outliers were small tumors (8/10 were smaller than 1,7 cm^2), laid in small bread loaves, and/or had low maximal fluorescence intensities. Therefore, it is assumed the cluster gave a correct representation of the real values

which are expected to be measured intraoperatively.

Furthermore, the clustering of the background fluorescence intensities in the bread loaves was found in the graph of the comparison with the maximal fluorescence intensity (*Figure 12A*). The graph showed the background fluorescence intensity was, in 84,8% of the cases (28/33), between 9,8% (25/255) and 21,6% (55/255) of the maximal fluorescence intensity. However, the spread in background fluorescence intensity values was still large (11,8%). Especially when taken into account that the data will be used to evaluate resection margins in millimeters or even smaller. Therefore, more research on the precise relation between background fluorescence intensity in the bread loaf and the maximal fluorescent intensity needs to be performed. The background fluorescent intensity in the bread loaf in a.u. correlates with the maximal fluorescent intensity in *Figure 12B*. Bread loaves with a higher maximal fluorescent intensity displayed higher background fluorescence intensities in the bread loaves. However, the background fluorescent intensity in the bread loaf was calculated by taking the mean fluorescent intensity in the whole bread loaf without the tumor tissue. Therefore, the mean includes the fluorescent halo around the tumor. However, as mentioned earlier, calculating the real background intensity in the bread loaf proved to be difficult.

The group including all bread loaves showed the highest values for the parameters 'mean', 'Q25', 'Q50', and 'Q75' in octants 3 and 7. This suggested higher fluorescent intensity values are expected around the CRLM when moving deeper into the liver compared to the fluorescence intensities at the liver surface around the CRLM. The histogram parameter 'mean' showed the highest values in the halo of 0,5 to 1 millimeter from the tumor in octants 3 and 7, and of 1 to 2 millimeters in octants 2 and 6 from the tumor. Therefore, the fluorescent rim is expected to have the highest fluorescent intensities close to the tumor which decreases after 1 or 2 millimeters depending on the perspective in which the bread loaf is imaged. A relatively high amount of low pixel intensity is expected in the bread loaves as the 'Q50' values were lower compared to the 'mean' values.

In this research, the bread loaves were divided multiple times into different groups to find the effect of patient- and tumor-specific characteristics.

Preoperative chemotherapy showed to have a negative effect on the maximal fluorescence intensity as bread loaves in the non-chemotherapy group showed significantly higher maximal fluorescent intensities. The other general parameters were similar for groups including patients who did or did not receive preoperative chemotherapy. The comparisons between the background fluorescence intensity in the bread loaves, tumors, and the maximal fluorescence intensity in the image supported the finding of the significantly higher maximal fluorescent intensities in the non-chemotherapy bread loaves. For both the comparisons of the background fluorescence intensities in the bread loaves and the tumor with the maximal fluorescence intensity, the non-chemotherapy and chemotherapy groups could be divided with some overlap in the middle of the graphs. Therefore, these findings suggest preoperative chemotherapy will lead to lower maximal fluorescence intensities.

Despite the groups differed in maximal fluorescence intensity, both groups did have a similar share in the datapoints positioned inside of the cluster in the comparison between both background fluorescence intensities. Therefore, preoperative chemotherapy showed to not affect the ratio of both background fluorescence intensities with the maximal fluorescence intensity.

Bread loaves from patients who did receive preoperative chemotherapy showed a

different distribution of the parameter value 'mean' compared to non-chemotherapy patients. These bread loaves showed a peak in the mean 'mean' fluorescence intensity farther away from the tumor. Therefore, preoperative chemotherapy will affect the distribution of ICG around CRLM and must be compensated to be able to predict the distance to the tumor.

Besides, the chemotherapy patients showed lower mean 'mean' values (in values between 0-255) for all octants in all halos. Combined with the lower maximal fluorescence intensity in a.u., this suggests preoperative chemotherapy will lead to less accumulation of ICG around the CRLM. Moreover, the signal-to-background ratio in the chemotherapy bread loaves will be lower as the background fluorescence intensity in the bread loaf (0-255) was similar for both groups and the mean 'mean' fluorescence intensity (0-255) lower in the chemotherapy group.

The accumulation of ICG around CRLM is assumed to be caused by the presence of immature hepatocytes around the CRLM with reduced bile excretion (15) as ICG is excreted by the biliary system. Chemotherapy causes a lower accumulation of ICG in the liver as well as a relatively lower accumulation around the CRLM. Therefore, chemotherapy is believed to affect the uptake of ICG in or excretion of ICG out of the liver. However, additional research is needed to find the reason for this difference in the accumulation of ICG after preoperative chemotherapy.

The capsular and subcapsular lesions did not show any significant differences in general parameters. However, the mean maximal fluorescence intensity (a.u.) in the images in subcapsular lesions was slightly lower and showed a lower spread in values. Furthermore, the datapoints from the subcapsular group showed a lower spread of datapoints over the maximal fluorescence intensity axis compared to the capsular group in the comparisons with both background fluorescent intensities. Therefore, the absolute accumulation of ICG in livers with subcapsular lesions is expected to be more predictable compared to the capsular lesions. Both types of lesions showed datapoints in the cluster of the comparison of both background fluorescence intensities (*Figure 19*. However, 42,1% (8/19) of the lesions of the capsular group were positioned outside of the cluster while the subcapsular group only had 20% (2/10) of their lesions positioned outside of the cluster. However, as mentioned before, most of the datapoints outside of the cluster laid in bread loaves with small tumors or in small bread loaves. Therefore, it is not expected that the type of lesion will affect both background fluorescence intensities.

An interesting observation between both types of lesions was the difference in the octants with the highest values for the parameter 'mean'. Capsular lesions showed the highest values in octants 3 and 7, the octants deeper into the liver, while subcapsular lesions showed the highest values for the parameter 'mean' in octants 2 and 6. Therefore, the highest accumulation of ICG around subcapsular lesions was observed in between the liver border and the tumor. However, the differences in the mean 'mean' fluorescence intensities in the different halos were smaller between the octants in the subcapsular lesions group compared to the capsular lesions group. Besides, the values of the parameter 'mean' were lower in subcapsular lesions group compared to the capsular lesions group. Concluding, capsular lesions showed less excretion or a higher uptake of ICG around the tumor deeper in the liver compared to subcapsular lesions. While subcapsular lesions had less excretion or a higher uptake of ICG between the liver border and the tumor compared to the side deeper in the liver of the subcapsular tumors.

Another interesting observation was the difference between both types of lesions in the distribution of the histogram parameter values over distance to the tumor. Subcapsular

lesions showed an increase in values up to the halos of 2 to 3 or 3 to 4 millimeters from the tumor for varying octants, while capsular lesions showed an increase up to the halo from 1 or 2 millimeters for most octants. This observation, combined with the lower peak in the mean fluorescence intensities of the histogram parameter 'mean', suggest subcapsular lesions have a different effect on the accumulation of ICG compared to the capsular lesions. Therefore, the type of lesion will affect the prediction of the resection margin. Besides, for both types of lesions, the perspective (front or back) from which the lesions were imaged will affect the expected accumulation of ICG around the tumor. Therefore, the perspective from which the tumor is imaged must also be considered for a correct prediction of the resection margin.

The effect of the size of the tumor on the general parameters was difficult to determine. The groups had a large variation in patient and tumor characteristics. However, the parameter background fluorescence intensity in the tumor did decrease with the increase of the size of the tumors. This finding supported the assumption that in smaller tumors it is possible to measure the fluorescence of ICG which is positioned behind the tumor tissue in the bread loaf and increases the background fluorescence intensity in the tumor.

The group with the largest tumors (>3 cm^2) did present a low spread of values in the graphs comparing one of both background fluorescence intensities with the maximal fluorescence intensity. Based on these findings it is assumed that it is possible to accurately predict the background fluorescence intensities for this group of tumors when the maximal fluorescence intensity is retrieved and vice versa. However, the three groups with tumors smaller than 3 cm^2 did show less clustering. Therefore, the prediction of the background fluorescence intensities based on the maximal fluorescence intensity will be less accurate for these three groups of tumors. The same is seen when comparing both background fluorescence intensities. It is surely possible to predict one of the two parameters, within an acceptable range, when the other parameter is retrieved for the group with the biggest tumors (>3 cm2). While the three groups with smaller tumors showed outliers for 33% of their datapoints and are, therefore, less predictable.

Despite the different groups of tumors were difficult to compare, the parameter 'mean' showed the highest values in octants 3 and 7 for almost all different halos in all four groups of tumors. The group with the largest tumors showed the highest parameter values farther away from the tumor compared to the other three groups of tumors. This suggests the size of the tumor could potentially affect the accumulation of ICG around the tumor. The group with the smallest tumors (0-1 cm^2) showed low 'mean' values. However, this could be caused by 'missing' data for these halos as most tumors laid in small bread loaves, and ink and cauterization affected the measurements.

In conclusion, it is difficult to predict the exact effect of tumor size on the distribution of ICG around the CRLM. More data is needed to be able to make a precise prediction about the effect of tumor size as this group did not include enough bread loaves to create generic groups. The only group which showed constant results was the group with tumors larger than 3 cm^2. For this group, it is expected the tumor size can be used as a predictive factor for the distribution of ICG around the tumor.

At last, the data found during this research was inserted in *Equation 2*. This showed maxima of predicted measured fluorescence intensities at around 5 millimeters from the tumor. As mentioned earlier, the formula gives a rough estimation for the expected values as it had its weaknesses. However, a peak intensity at around 5 millimeters from the tumor is feasible. The photons are expected to move a mean of 4,68 millimeter through liver tissue

and the mean fluorescence intensity decreased after the halo from 0,5 to 1 millimeter from the tumor.

The distribution of the expected measured values showed the potential of the use of peritumoral rim as an indicator for the resection margin. However, development to improve the calculation method is needed to be able to predict resection margins. Moreover, the outcomes of this method must be compared to values which are measured in the operation room.

The formula used the mean fluorescence intensity of a whole halo in an octant to calculate the expected measured fluorescence intensity. However, intraoperatively, the mean fluorescence intensity must be calculated over smaller areas to accurately predict the smallest margin to the tumor. This makes the prediction of the resection margin more challenging as the smaller area will be affected by the high variation in pixel intensities. Therefore, areas, which are large enough to compensate for the variation in pixel intensities, must be selected to be able to make accurate predictions of the distances to the tumor.

Theoretically, based on the findings of this research, it is not impossible to predict the resection margin with the use of the fluorescence of ICG which accumulated around CRLM. However, several improvements and additions must be made to this research to be able to make the prediction of the resection margin. Several potential improvements are already mentioned in this section. However, these improvements completed by additional potential improvements will be further discussed in the section 'Future recommendations'.

Conclusion

This research aimed to investigate the possibility to use the fluorescent rim around CRLM to evaluate resection margins intraoperatively. Based on the findings of this research, there is no reason to assume it is not possible to develop a predictive model using the fluorescent rim to evaluate resection margins during surgery.

This research showed that the background fluorescence intensity in the liver and in the tumor (in units between 0 and 255) were related to the maximal fluorescence intensity in a.u. and were constant between patients. Therefore, these parameters can be used to calibrate a predictive model. Besides, the effects of preoperative chemotherapy, the location of the CRLM, and the size of the CRLM on the distribution of ICG around CRLM were shown. Therefore, the model must correct for .

the patient and tumor characteristics. Moreover, more data should be obtained to expand the database to increase the accuracy of the data analysis. Besides, a method to generate 'ground truth' delineations of CRLM in images generated with the PEARL imaging system must be developed to increase the accuracy of the data generation in MeVisLab. At last, the findings of this research must be validated in the operation room. This will show the usability of the fluorescent rim around CRLM to evaluate resection margins.

In conclusion, the peritumoral fluorescent rim of ICG around CRLM could potentially be used as a predictive factor for resection margins. However, additional research must be performed to be able to develop an accurate predictive model.

Future recommendations

This research showed the potential of the fluorescent rim. However, to be able to develop an accurate predictive model several steps must be taken. This section will elaborate about the steps that must be taken. Moreover, several more recommendations will be made regarding future research.

Implementation plan

This research aimed to investigate the possibility to develop a model which can be used to evaluate resection margins. Effects of several tumor and patient characteristics on the peritumoral fluorescent rim were shown as the distribution of ICG around CRLM was analyzed. However, before further development of this method, an implementation plan should be written. This plan should focus on the possibilities to intraoperatively image the resected samples and answer questions such as, 'Will the PEARL imaging system or the Quest camera be used to evaluate the resection margin?', 'How will the resected samples be imaged?', 'How can the whole resected sample accurately be evaluated during surgery?', 'What are the possibilities to calibrate calculations during surgery?', and 'Will the sample be imaged in whole or after the sample is cut in bread loaves?'. These are only examples of questions which must be answered before the next steps in this research should be taken. The answers on these questions will have a great influence on how the data must be processed, what kind of new data is needed to be generated, and how the predictive model should work. Therefore, an implementation plan must be written to optimize the research activities.

Intraoperative imaging method

An important decision, which must be made in the implementation plan, is the decision on how the resected sample will be imaged during surgery to predict the resection margin. A standardized method is not yet used and therefore needs to be designed. This method must be capable to be standardized and repeatable for all tumors. One of the possibilities lays in a camera which can move around the resected tumor. A camera which can rotate around the resected tumor with the tumor as origin would be an ideal option. In this way the whole specimen can be examined to determine the exact location where the margin between resection plane and tumor is the smallest. The same distance needs to be capped to the sample as the measured fluorescence intensities will vary when varying in distance to the tumor. However, this problem could be solved by compensating for variations in distance to the resected sample.

Development of the database

The development of the data and data analysis is an important next step following the conclusions of this research. An expansion of the database will contribute to generate better comparable groups when characteristics are compared with each other. Eventually the database must be expanded with more tumor and patient characteristics to investigate more potential prognostics factors for the distribution of ICG around CRLM.

Moreover, a new group of bread loaves must be generated. This new group must include bread loaves with sufficient liver tissue around the tumor to fill all octants. This will lead to a more completed database and therefore a better understanding on the exact distribution of ICG around CRLM. Naturally, an exception must be made for capsular lesions. The analysis of this new group of bread loaves will contribute to interpret the data analysis of groups containing tumors where not all octants are filled with liver tissue.

Generation of ground truth images from the PEARL images

As mentioned at the interobserver section, there is a need for ground truth delineations of CRLM in PEARL images. Therefore, a new and special protocol to enclose and examine CRLM must be developed for histological research. The histological margins must be compared with the delineations from the tumor in the PEARL images. This comparison will contribute to add accuracy to the calculations, as well as contribute to revalue the mean histogram parameters found in this research.

Development of the MeVisLab network (data generation)

The MeVisLab network used in this research can be improved to decrease the chance of missing data. The first development should be the change from octants to quadrants. This research did not include the results from octants 1, 4, 5, and 8 as for most tumors data was missing in these four octants. This will be prevented when changing the octants to quadrants (*Figure 30A*).

The octants should have provided an increase in information about the distribution of ICG around the tumor. However, because of missing data, the octants could not show their potential. An option to gain more information about the distribution of ICG then by using quadrants alone could be dividing these quadrants by adding a diagonal line between the corner of the quadrant in the middle of the tumor and the corner farthest outside of the tumor (*Figure 30B*). This could add information about the distribution around the tumor and is expected to be less sensitive for missing data.

Another improvement of the MeVisLab network could be the increase in the number of halos used. The calculations of the expected measured fluorescence intensities showed a peak between 5 and 10 millimeters from the tumor. By adding the halos of 5 to 6, 6 to 7, 7 to 8, 8 to 9, and 9 to 10 millimeters from the tumor a more precise prediction of the expected measured values can be performed.

Development of the calculation method

This research used a formula which used the mean fluorescence intensity in different halos as a variable to give a rough estimation of the expected measured fluorescence intensities at various distances to the tumor. To improve the accuracy of the calculation, and to decrease the dependency on one specific parameter, a

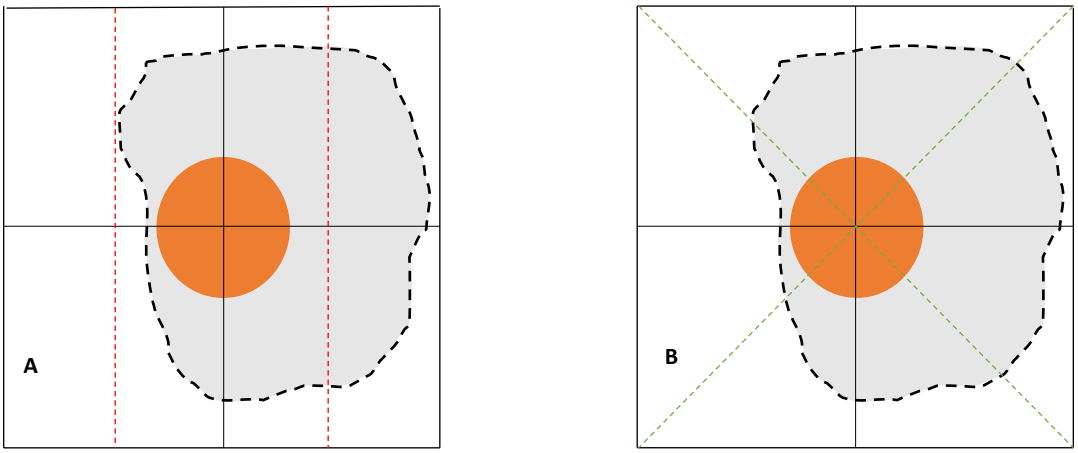

Figure 30 *- Alternative for the initial octants*

The orange circle shows a tumor, and the grey area shows the imaged bread loaf. (A) shows the initial octants. After deleting the red dashed lines quadrants are created. (B) shows an alternative for the octants used in this research. The dashed green lines will be added to the quadrants so eight triangles are created. As displayed, this alternative will prevent cases of missing data.

combination of parameters could be used to evaluate the resection margin. The combination of parameters will improve the calculations' robustness what is needed for images with a high variation in pixel intensities. Every different parameter analyzed in this research showed a unique distribution of its values over distance from the tumor. Therefore, a combination of more parameters could be an option to consider. However, the calculations will get more complicated and therefore will demand more computational power what will slow down the calculations. Thus, a trade-off must be made between the speed of the calculations and the accuracy of the calculations.

Correlation between intraoperatively measured values and values measured during research

An important next step would be to translate the findings of this research to real imaging in the operation room. The implementation plan will provide the method how the resected specimen will be imaged in the operation room. However, before finishing the implementation plan, the calculation method can already be checked with the use of the PEARL. By landmarking specific areas and imaging the specimen in whole in the PEARL, there will be an opportunity to cut the sample in bread loaves at those specific landmarks. In this way one should be able, in combination of the new enclosing and examining protocol for CRLM, to measure the resection margin at that specific point. The fluorescence intensity measured at this specific point can then be correlated with the findings of this research. This will lead to a better understanding of the real measured fluorescence intensities which are expected to measure intraoperatively.

In conclusion, several potential steps can be taken to improve this research and contribute to build towards real-time tumor margin assessment in colorectal liver metastases surgery using near-infrared fluorescence-imaging.

References

1. Volksgezonheid en zorg. Huidige cijfers dikker darm kanker Nederland. 2021.
2. van der Geest LG, Lam-Boer J, Koopman M, Verhoef C, Elferink MA, de Wilt JH. Nationwide trends in incidence, treatment and survival of colorectal cancer patients with synchronous metastases. Clin Exp Metastasis. 2015;32(5):457-65.
3. Oncoline. Diagnostiek en behandeling van colorectale levermetastasen. 2021.
4. Engstrand J, Nilsson H, Strömberg C, Jonas E, Freedman J. Colorectal cancer liver metastases - a population-based study on incidence, management and survival. BMC Cancer. 2018;18(1):78.
5. Hackl C, Neumann P, Gerken M, Loss M, Klinkhammer-Schalke M, Schlitt HJ. Treatment of colorectal liver metastases in Germany: a ten-year population-based analysis of 5772 cases of primary colorectal adenocarcinoma. BMC Cancer. 2014;14:810.
6. Ferlay J, Shin HR, Bray F, Forman D, Mathers C, Parkin DM. Estimates of worldwide burden of cancer in 2008: GLOBOCAN 2008. Int J Cancer. 2010;127(12):2893-917.
7. Venkat SR, Mohan PP, Gandhi RT. Colorectal Liver Metastasis: Overview of Treatment Paradigm Highlighting the Role of Ablation. AJR Am J Roentgenol. 2018;210(4):883-90.
8. Chow FC, Chok KS. Colorectal liver metastases: An update on multidisciplinary approach. World J Hepatol. 2019;11(2):150-72.
9. Ardito F, Panettieri E, Vellone M, Ferrucci M, Coppola A, Silvestrini N, et al. The impact of R1 resection for colorectal liver metastases on local recurrence and overall survival in the era of modern chemotherapy: An analysis of 1,428 resection areas. Surgery. 2019;165(4):712-20.
10. Kraft JC, Ho RJ. Interactions of indocyanine green and lipid in enhancing near-infrared fluorescence properties: the basis for near-infrared imaging in vivo. Biochemistry. 2014;53(8):1275-83.
11. Handgraaf HJM, Boogerd LSF, Höppener DJ, Peloso A, Sibinga Mulder BG, Hoogstins CES, et al. Long-term follow-up after near-infrared fluorescence-guided resection of colorectal liver metastases: A retrospective multicenter analysis. Eur J Surg Oncol. 2017;43(8):1463-71.
12. Shinohara H, Tanaka A, Kitai T, Yanabu N, Inomoto T, Satoh S, et al. Direct measurement of hepatic indocyanine green clearance with near-infrared spectroscopy: separate evaluation of uptake and removal. Hepatology. 1996;23(1):137-44.
13. Ishizawa T, Fukushima N, Shibahara J, Masuda K, Tamura S, Aoki T, et al. Real-time identification of liver cancers by using indocyanine green fluorescent imaging. Cancer. 2009;115(11):2491-504.
14. van Manen L, Handgraaf HJM, Diana M, Dijkstra J, Ishizawa T, Vahrmeijer AL, et al. A practical guide for the use of indocyanine green and methylene blue in fluorescence-guided abdominal surgery. J Surg Oncol. 2018;118(2):283-300.
15. van der Vorst JR, Schaafsma BE, Hutteman M, Verbeek FP, Liefers GJ, Hartgrink HH, et al. Near-infrared fluorescence-guided resection of colorectal liver metastases. Cancer. 2013;119(18):3411-8.
16. Poon RT, Fan ST, Wong J. Liver resection using a saline-linked radiofrequency dissecting sealer for transection of the liver. J Am Coll Surg. 2005;200(2):308-13.
17. Bankhead P, Loughrey MB, Fernández JA, Dombrowski Y, McArt DG, Dunne PD, et al. QuPath: Open source software for digital pathology image analysis. Scientific Reports. 2017;7(1):16878.
18. Saccomandi P, Vogel V, Bazrafshan B, Maurer J, Schena E, Vogl TJ, et al. Estimation of anisotropy coefficient of swine pancreas, liver and muscle at 1064 nm based on goniometric technique. J Biophotonics. 2015;8(5):422-8.
19. Hafeez U, Atif M, Firdous S, Mehmood MS, Hamza MY, Imran M, et al. Optical properties of normal and thermally coagulated chicken liver tissue measured ex-vivo with diffuse reflectance. Optics and Spectroscopy. 2011;110(2):313-9.

Appendix

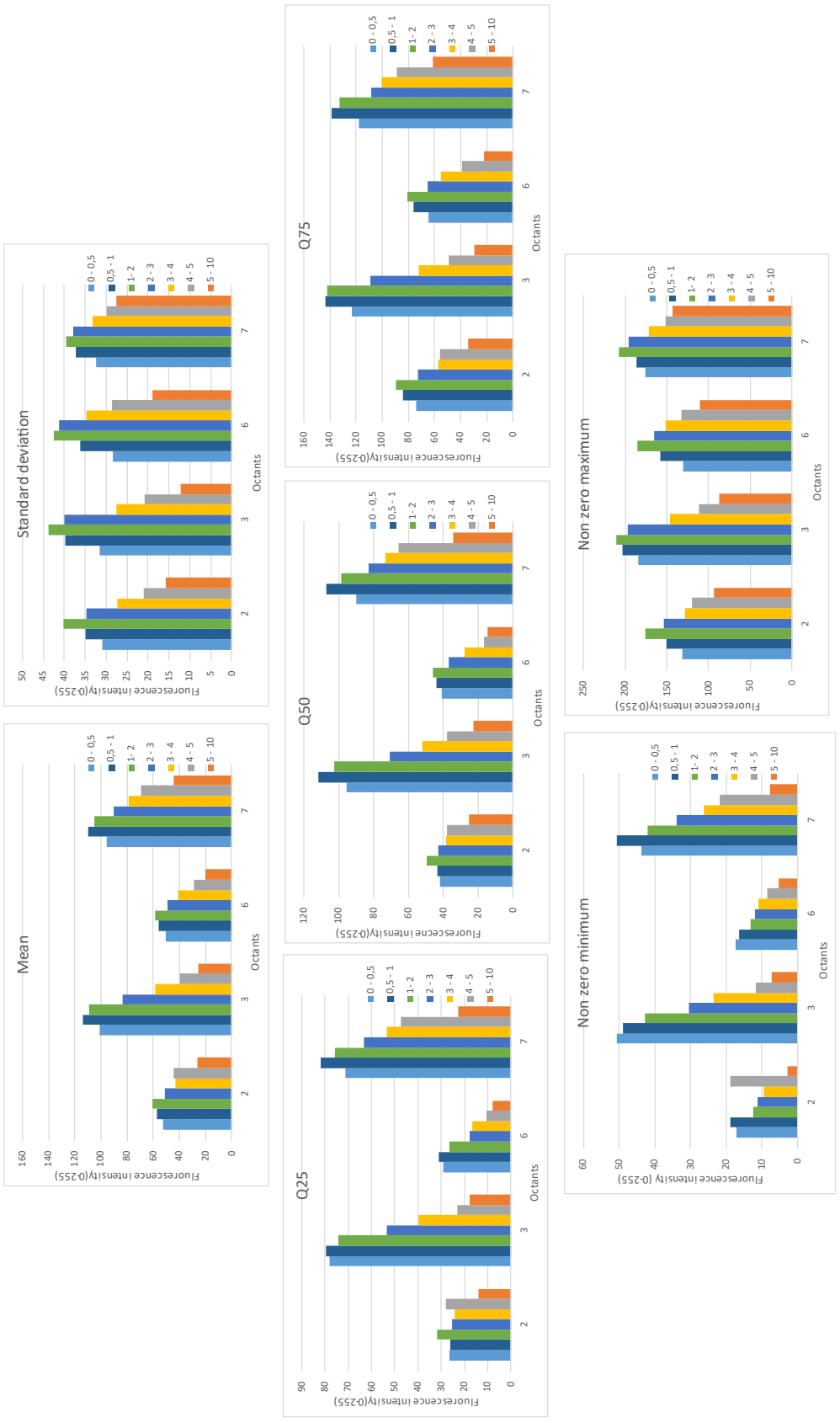

***Appendix A** - Results of the histogram parameters for the different fluorescent halos of the preoperative chemotherapy group*

***Appendix B** - Results of the histogram parameters for the different fluorescent halos of the non-chemotherapy group*

Universiteit Leiden The Netherlands

TU Delft Delft University of Technology

Erasmus University Rotterdam

***Appendix C** - Results of the histogram parameters for the different fluorescent halos of the capsular lesions group*

***Appendix D** - Results of the histogram parameters for the different fluorescent halos of the subcapsular lesions group*

Universiteit Leiden The Netherlands

TU Delft Delft University of Technology

Erasmus University Rotterdam

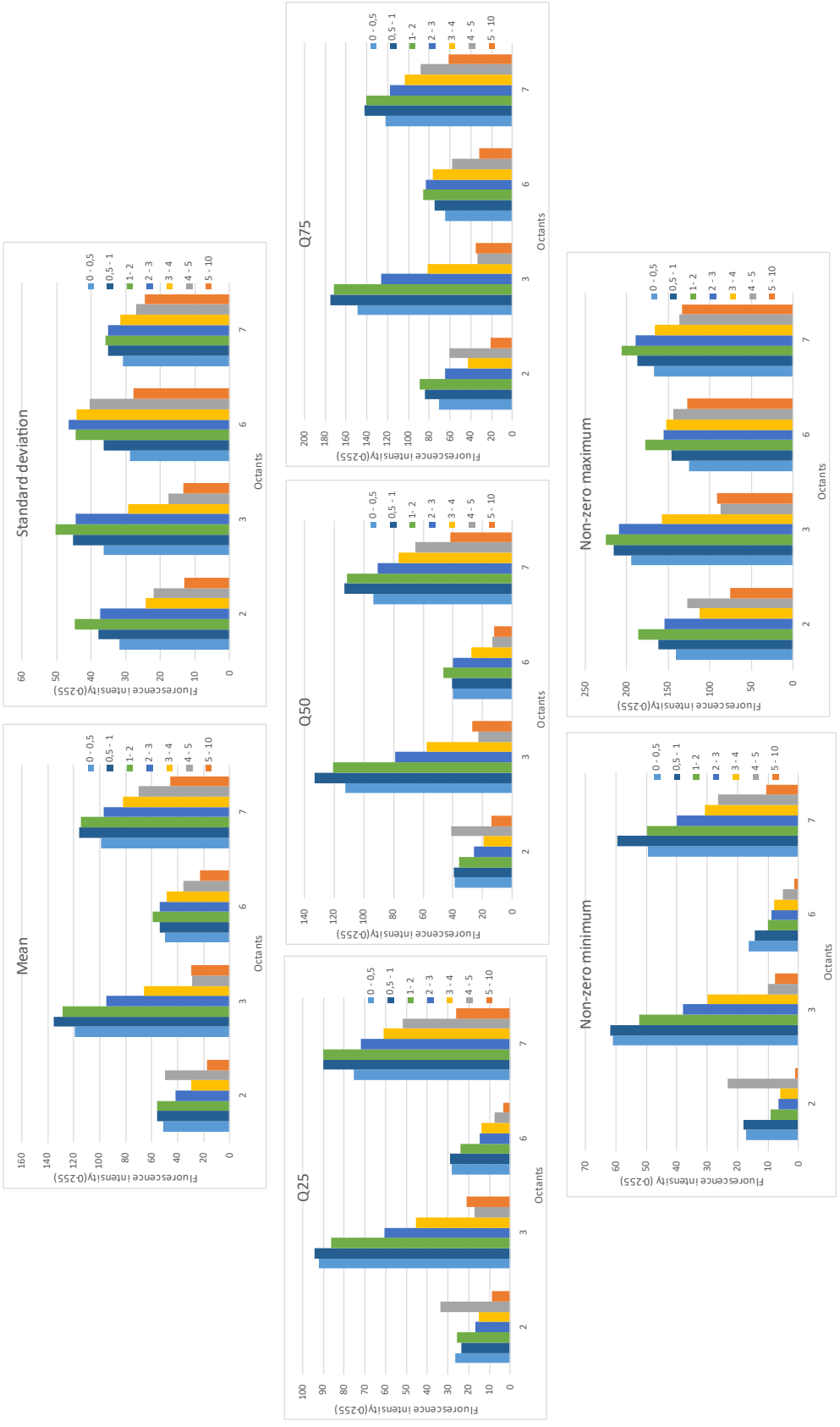

***Appendix E** - Results of the histogram parameters for the different fluorescent halos of the lesions between 0 and 1 cm² group*

***Appendix F** - Results of the histogram parameters for the different fluorescent halos of the lesions between 1 and 2 cm^2 group*

Universiteit Leiden The Netherlands

TU Delft Delft University of Technology

Erasmus University Rotterdam

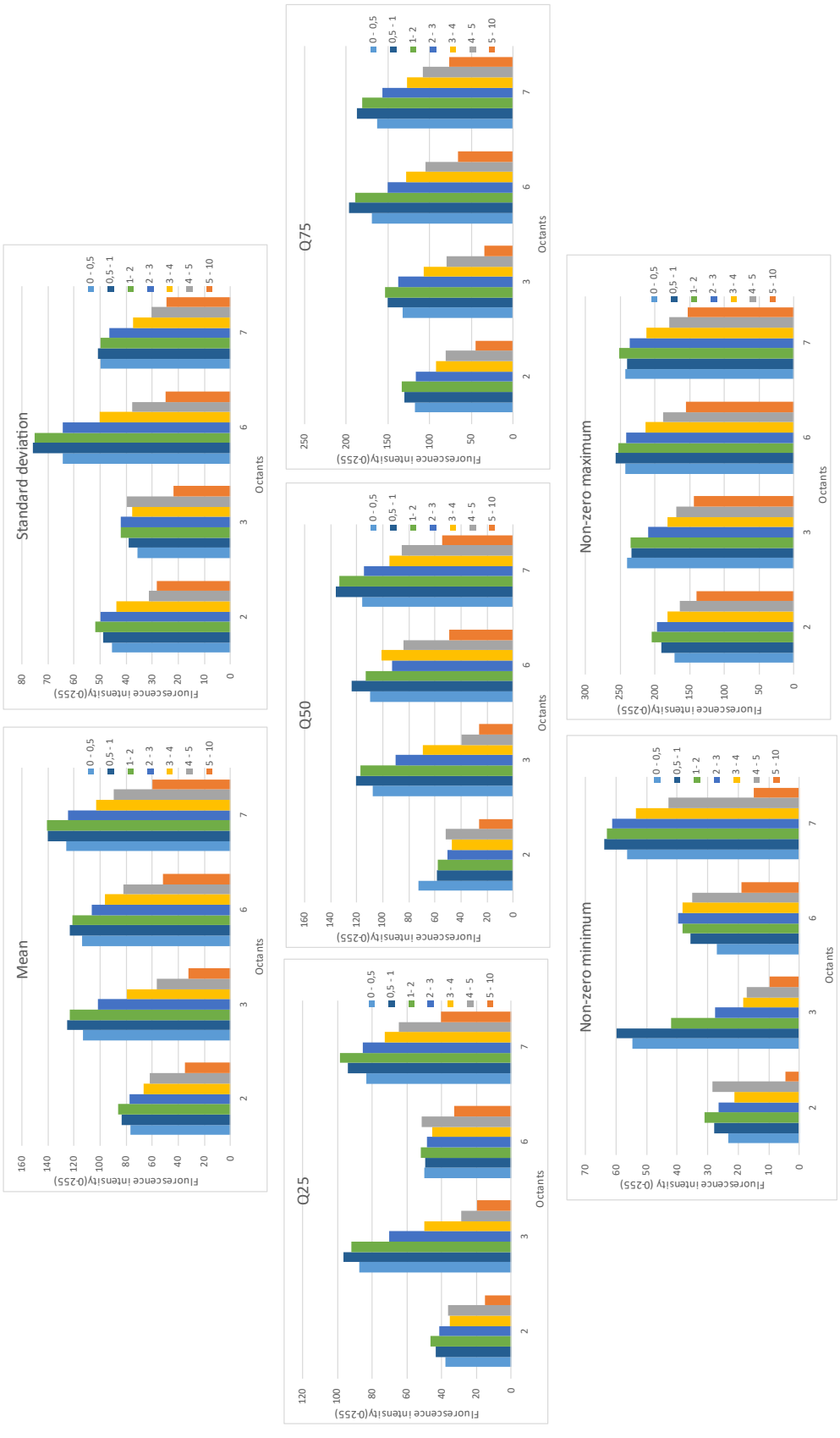

***Appendix G** - Results of the histogram parameters for the different fluorescent halos of the lesions between 2 and 3 cm^2 group*

***Appendix H** - Results of the histogram parameters for the different fluorescent halos of the lesions larger than 3 cm² group*